PPSP-UBLS-82-3

A SIMULATION MODEL OF RIVER FLOW AND DO DYNAMICS DOWNSTREAM OF CONOWINGO DAM

Prepared by

ENVIRONMENTAL CENTER
Martin Marietta Corporation
1450 South Rolling Road
Baltimore, Maryland 21227-3898

COASTAL ZONE

INFORMATION CENTER

Prepared for

Maryland Department of Natural Resources
Power Plant Siting Program
Tawes State Office Building
Annapolis, Maryland 21401

December 1982

MARYLAND POWER PLANT SITING PROGRAM

NATURAL RESOURCES ■ DEPARTMENT OF HEALTH AND MENTAL
EPARTMENT OF ECONOMIC AND COMMUNITY DEVELOPMENT ■ DE-
TATE PLANNING ■ DEPARTMENT OF TRANSPORTATION ■ DEPART-
ULTURE ■ COMPTROLLER OF THE TREASURY ■ PUBLIC SERVICE

Maryland Dept of Natural Resources

GB
1207
.D99
1982

MD
W.P.

PPSP-UBLS-82-3

A SIMULATION MODEL OF RIVER FLOW AND DO DYNAMICS DOWNSTREAM OF CONOWINGO DAM

COASTAL ZONE
INFORMATION CENTER

Robert L. Dwyer
Martha A. Turner

ENVIRONMENTAL CENTER
Martin Marietta Corporation
1450 South Rolling Road
Baltimore, Maryland 21227-3898

GB1207 .D99 1982

Approval for Release:

W. A. Richkus
Technical Director
Site Evaluation

T. T. Polgar
Associate Director

December 1982

FOREWORD

This report describes the development of a model which simulates river flow and dissolved oxygen dynamics in the Susquehanna River between Conowingo Dam and the limit of tidal influence at the fall line. This study is one component of a research program on the impact of Conowingo Dam operations funded by the Maryland Power Plant Siting Program. Other work is being carried out by contractors for Philadelphia Electric Company.

Martin Marietta Environmental Center (EC) serves as Biological Integrator for the Site Evaluation Division under Contract P20-83-03 from the Maryland Power Plant Siting Program, Department of Natural Resources. This report has been prepared in compliance with the contractual requirements set forth in the EC's statement of work, and it is being released for public distribution.

Peter M. Dunbar
Administrator
Site Evaluation

ABSTRACT

The hydroelectric plant in Conowingo Dam on the Susquehanna River (Maryland) operates on a cyclic daily schedule which results in fluctuations in downstream flow and water level. Downstream dissolved oxygen (DO) concentration also fluctuates daily. Low DO concentrations can reduce the value of the downstream river reach as habitat for fish and invertebrates. Consequently, a numerical model was developed to quantify the relative contributions to DO distributions downstream of the dam of:

- The DO water discharged by the turbines (controlled by discharge and by processes in the reservoir),
- Metabolism of oxygen by the water column and benthic communities, and
- Physical processes in the river reach (such as atmospheric reaeration).

The model structure is based on an existing one-dimensional hydrodynamic model capable of simulating unsteady flows, and is coupled to differential equations for oxygen dynamics, which include mechanisms for the factors described above. The hydrodynamic portion of the model was calibrated and validated using data sets for dam discharge and water surface elevations from two separate time intervals. The DO segment of the model was calibrated using field measurements of metabolic rates and reaeration, and was validated against observed DO concentration measured at the downstream model boundary. Sensitivity analyses revealed the following order of importance for in situ processes: benthic oxygen production, atmospheric diffusion, benthic respiration, water-column community production, and water-column respiration. Model simulations revealed that at high discharges (28,000-40,000 cfs), the DO of the discharge contributed 85-90% of the oxygen crossing the downstream boundary (i.e., leaving the system). Most of the remainder is due to atmospheric reaeration. At discharges below 5000 cfs, downstream DO is controlled by the DO of the dam discharge (66%), whereas the remainder is due mostly to benthic metabolism.

TABLE OF CONTENTS

		Page
FOREWORD		iii
ABSTRACT		v
I.	INTRODUCTION	I-1
II.	DEVELOPMENT OF A HYDRODYNAMIC SIMULATION MODEL OF THE SUSQUEHANNA RIVER BELOW CONOWINGO DAM	II-1
	A. DESCRIPTION OF THE PROBLEM AND GENERAL APPROACH	II-1
	B. APPROACH TO HYDRODYNAMIC MODELING	II-3
	C. CALIBRATION OF USTFLO TO OBSERVED FLOW DATA	II-14
	D. VALIDATION OF USTFLO	II-18
III.	MODEL OF DISSOLVED OXYGEN DYNAMICS	III-1
	A. BACKGROUND	III-1
	B. DIFFERENTIAL EQUATION DESCRIBING OXYGEN RATE OF CHANGE	III-1
	C. NONCONSERVATIVE PROCESSES AFFECTING DO IN THE RIVER REACH: ESTIMATION OF RATES FOR INCLUSION IN THE DO MODEL	III-11
	D. CALIBRATION OF PARAMETERS IN THE DO MODEL	III-31
	E. VALIDATION OF THE DO MODEL	III-38
	F. RELATIVE CONTRIBUTIONS OF INDIVIDUAL RATES TO SIMULATED DO	III-50
	G. SENSITIVITY ANALYSIS	III-52
	H. DISCUSSION	III-58
IV.	LITERATURE CITED	IV-1

TABLE OF CONTENTS (CONTINUED)

	Page
APPENDIX A	
SATURATED DO CONCENTRATION OF WATER (FROM KESTER 1975).....	A-1
APPENDIX B	
ESTIMATION OF DIEL TEMPERATURE CHANGES IN RIVER SEGMENTS.....	B-1
APPENDIX C	
REGRESSION OF WATER COLUMN RESPIRATION VS. TEMPERATURE.....	C-1
APPENDIX D	
REGRESSION OF BENTHIC RESPIRATION VS. TEMPERATURE.....	D-1
APPENDIX E	
CALCULATION OF SOLAR RADIATION AT THE WATER SURFACE FROM ASTRONOMICAL AND METEOROLOGICAL INFORMATION.....	E-1
APPENDIX F	
NONLINEAR REGRESSIONS FITTING WATER-COLUMN METABOLISM DATA TO THE STEELE (1965) EQUATION..	F-1

LIST OF TABLES

Table No.		Page
II-1	Geometric parameters for 5 model transects at different water elevations.....	II-11
III-1a	River dispersion coefficients (from dye release on 26 August and 2 September 1981).	III-7
III-1b	Model dispersion coefficients (from model simulations at steady-state flows using 2 September 1981 hydrodynamic data).....	III-9
III-2	Estimates of average differences between simulated and actual values for system outputs for three validation runs.....	III-41
III-3	Relative contributions of individual rate processes (%) of the concentrations of DO for two periods.....	III-47
III-4	Sensitivity of simulated output DO to artificial variations of oxygen rate processes.....	III-54
III-5	Sensitivity of simulated output DO to artificial variations of system inputs.....	III-57

LIST OF FIGURES

Figure No.		Page
II-1	Susquehanna River between Conowingo Dam and the fall line, showing longitudinal segmentation.....	II-9
II-2	Stage-discharge rating curves used by USTFLO.....	II-15
II-3	Measured and simulated water surface elevations along the river reach for three steady-state flows.....	II-17
II-4	Initial hydrodynamic calibration run, using constant Manning bottom friction coefficients.....	II-19
II-5	Validation of hydrodynamic model, 8-10 July 1981 - simulated water surface elevations at five USTFLO transects.....	II-20
II-6	Validation of hydrodynamic model, 8-10 July 1981 - simulated water surface elevations at five USTFLO transects.....	II-22
III-1	Typical time-concentration record from a river station during downstream transport of a dye mass released at the dam.....	III-6
III-2	Simulated time-concentration curves at four downstream transects during a discharge of 3,500 cfs.....	III-8
III-3	Reaeration coefficient as a function of discharge.....	III-13
III-4	Estimates of respiration of water-column community, April-October 1980.....	III-16
III-5	Estimates of respiration of water-column community vs. distance from Conowingo Dam (meters).....	III-17
III-6	Respiration of water-column community vs. temperature.....	III-18

LIST OF FIGURES (CONTINUED)

Figure No.		Page
III-7	Means of replicate benthic respiration measurements by transect and hydrologic habitat type.....	III-20
III-8	Means of replicate benthic respiration measurements by transect and hydrologic habitat type.....	III-21
III-9	Benthic community respiration vs. temperature.....	III-23
III-10	Estimated net production of water-column community April-October 1980.....	III-26
III-11	Gross oxygen production vs. estimated average light intensities at the depth and time of light-dark bottle incubations.....	III-28
III-12	Gross oxygen production of the benthic community vs. temperature.....	III-30
III-13	Calibration of the DO model, 5-7 July 1980.	III-33
III-14	Sensitivity over a day of simulated benthic oxygen production to different values of I_{opt} and Secchi-disk depth.....	III-35
III-15	Validation of the DO model for the continuous discharge period, 27-28 June 1981.....	III-40
III-16	Validation of the DO model, 25 July-2 August 1981.....	III-44
III-17	Validation of the DO model, 8-10 July 1980.	III-49

I. INTRODUCTION

Conowingo Dam, located 10 mi upstream of the mouth of the Susquehanna River in Maryland, contains a peaking-power hydroelectric plant which generates during times of peak daily power demand, and shuts down during periods when demand is low. Water levels downstream of the dam fluctuate in response to this cycle, and dissolved oxygen (DO) concentrations in the river each also show pronounced daily variations. Since low DO concentrations can have deleterious effects on a wide variety of aquatic life (Davis, 1975), the model described in this report was prepared in order to quantify the hydrodynamics and DO dynamics below the dam, and their relationship to dam discharge. This model is one component of a comprehensive set of studies of Conowingo Reservoir, the nontidal river reach below the dam, and the influence of the hydroelectric turbines as the connection between the two. The ultimate objective of the overall Conowingo program is the development of a set of measures which can be recommended to correct or mitigate low DO problems in the Susquehanna River below Conowingo Dam. Toward this end, the river model presented in this report will later be integrated with the analyses of the other segments of the reservoir and river system to provide a comprehensive assessment of the causes of the water quality problems, and to test the effects of some proposed alterations of the dam's operating schedules that are intended to improve habitat for fish and other biota.

This report specifically describes the formulation and validation of a hydrodynamic and DO simulation model for the river reach downstream of the dam. The model was calibrated using field data on flow and oxygen rate processes from the river reach. Model simulations quantify the relative contributions of

- the DO of the water discharged by the turbines (controlled by discharge and by processes in the reservoir),
- biological production and consumption of oxygen in the river reach, and
- physical processes in the river reach

on DO distributions downstream of the dam.

Development of this model is the first step in quantifying the processes affecting DO of the complete reservoir and free-flowing river segment influenced by the operations of Conowingo Dam.

II. DEVELOPMENT OF A HYDRODYNAMIC SIMULATION MODEL OF THE SUSQUEHANNA RIVER BELOW CONOWINGO DAM

A. DESCRIPTION OF THE PROBLEM AND GENERAL APPROACH

Available data (Philipp and Klose 1981; Carter 1973) indicate that summertime DO and temperature distributions downstream of Conowingo Dam are affected by fluctuations in the discharge of the turbines. Their major observations are the following:

- During periods of normal discharges, DO and temperature distributions in the reach are strongly influenced by the DO and temperature of the discharge water (which are controlled by the reservoir ecosystem combined with the patterns of water withdrawal associated with the turbines).
- During periods of turbine shutdown or low river discharges, the oxygen metabolism of the water-column, benthic, and fish communities in the river reach affect DO dynamics, and the intensity of solar heating controls distributions of water temperature.

State and federal resource agencies have suggested a con tinuous minimum discharge of water from Conowingo Reservoir as one possible means of improving aquatic habitat below the dam. In the reservoir, continuous vertical mixing (driven by a continuous discharge) might increase the DO at the depth of the turbine intakes (analyses of such effects on the reservoir will be the subject of a separate report). In the downstream reach, continuous flushing could reduce the amplitudes of daily fluctuations in DO and temperature. The amount of release, if any, necessary to achieve that objective is not yet known, but it might be possible to estimate the amount of such a release, either from available data or from the results of simulations from this or other models of the system.

We considered a number of analytical methods that could be applied to data collected by Maryland Power Plant Siting Program

(PPSP) studies in 1980 (Philipp and Klose 1981) and 1981 (Potera et al. 1982), and by studies for Philadelphia Electric Company (PECO) since 1970. One possible approach would be to apply statistical hypothesis testing (based on ANOVA methods) to the DO measurements made for a number of different discharge volumes in 1980 (e.g., to test the hypotheses that factors such as discharge volume, natural river flow, date of sampling, or sampling location affect DO). However, such analyses cannot identify mechanisms causing the variations in DO, and it is necessary to identify and quantify such mechanisms under present conditions before effects of future minimum discharge regimes can be predicted. In addition, statistical analyses would apply only to the period during which the field measurements were made and would have no predictive ability.

Another approach would be to use statistical time-series analyses to compare long-term records of upstream vs. downstream DO, or to forecast downstream values of DO based on the past history of discharge and DO. While time-series analyses permit the extrapolation of conditions for a short time into the future (based on the assumption that future statistical relationships will be very similar to those observed in the past), they cannot produce acceptable DO forecasts in the face of unpredictable natural changes of the system (e.g., wind-driven mixing events which eliminate DO stratification in the reservoir), or of man-made changes (e.g., planned modifications of the dam's discharge regime). In spite of these limitations, such analyses can provide some information on the interrelationships of discharge and DO distributions. We are presently completing time-series and other analyses of continuous DO, current, and wind data from the reservoir, taken in the summer of 1981 under conditions of normal peaking operations (Dwyer et al., in preparation).

A third method (and the one employed in this report) is deterministic simulation of the hydraulics and DO dynamics of the river reach of interest. This approach involves the numerical solution of differential equations describing the mechanics

of water flow, as well as the biogeochemical tranformations affecting DO in the river reach. This technique permits us to hypothesize mechanisms that affect DO, and to test their validity against observed data.

Once properly validated, such a model can be used to simulate flow and DO dynamics under hypothetical discharge regimes or other management strategies. The major disadvantages of this method are the amount of field data required for calibration and validation, the complexity of the computations, and errors arising from the degree of simplification of the model. However, since we need to quantify the factors affecting DO and to forecast DO distributions under discharge regimes that have not been observed in the field, the development and use of a mathematical model is the best method for this analysis.

The model described here deals only with oxygen dynamics in the river below the dam and thus addresses only one of the major aspects of the DO problem. We are currently studying oxygen dynamics in Conowingo Reservoir, and the source of water discharged by the turbines, and will discuss that work in future reports.

B. APPROACH TO HYDRODYNAMIC MODELING

The simulation of oxygen dynamics in the river below the dam first requires the development of a numerical model that reproduces the hydrodynamics in that river reach. Equations describing the conservation of momentum, plus an equation of continuity (conservation of mass), provide a complete description of water flow. The equations for one-dimensional flow in an open channel (the so-called Saint-Venant equations) are as follows:

$$\text{Continuity:} \quad \frac{\partial (AU)}{\partial x} + B \frac{\partial h}{\partial t} - q = 0 \qquad \text{(Eq.1)}$$

$$\text{Momentum:} \quad \frac{\partial h}{\partial x} + \frac{U}{g} \frac{\partial U}{\partial x} + \frac{1}{g} \frac{\partial U}{\partial t} + \frac{1}{g} \frac{q}{A} U = S_f \qquad \text{(Eq.2)}$$

where

A = cross-sectional area of flow, ft^2

U = mean velocity, ft/s

x = distance along channel, ft

B = water surface width, ft

h = water surface elevation above MSL, ft

t = time, s

g = acceleration of gravity, ft/s^2

q = tributary inflow per unit length along channel, $ft^3/s\text{-}ft$

S_f = friction slope = $\dfrac{n^2 U|U|}{2.21\ R^{4/3}}$ (where n = Manning n-value and R = hydraulic radius).

For applications where great precision in the solution in time or space is not needed, the equations can be simplified by eliminating one or more terms. However, since river flows downstream of Conowingo Dam are characterized by rapid fluctuations due to the peaking generation cycle, the present analyses require the solution of the complete equations. We chose a one-dimensional representation of the river due to the limitations of available biological and physical data. This representation limits the accuracy of the model in reproducing the spatial distributions of variables.

Choice of a General Hydrodynamic Modeling Program

The Saint-Venant equations (Eqs. 1 and 2) provide an exact description of one-dimensional flow in a river reach. Practical solution of the equations requires some numerical method. Two general classes of numerical solution schemes -- finite element methods and finite difference methods -- are in wide use today, and a number of generalized computer modeling packages using

these schemes are available to solve the Saint-Venant equations; they require only stream-specific parameters such as channel geometry and river flow. Two readily available computer model packages were selected for preliminary testing:

- SHP (Stream Hydraulics Package of WQRRS -- Water Quality for River-Reservoir Systems; Smith 1978), which uses a finite element method, and
- USTFLO (Unsteady Flow Hydrodynamics; HEC 1977), which uses a finite difference method.

Both models are distributed by the Hydrologic Engineering Center (HEC) of the U.S. Army Corps of Engineers. Initial simulation runs with SHP showed numerical instability (lack of convergence of model outputs), apparently caused by the package's inability to account for negative slope values for the river bottom (downward in the upstream, rather than the downstream, direction). Such negative slope values characterize the excavated tailrace pool immediately below the dam. In contrast, preliminary simulations of the Susquehanna River below Conowingo Dam using USTFLO showed no stability problems, and appeared to closely reproduce observed downstream flow responses to unsteady discharges. Thus, we chose USTFLO as the working tool for simulating river hydrodynamics. However, unlike the hydrodynamic modules of the SHP package, USTFLO does not have an associated water quality module to which it can be coupled. Therefore, we had to develop a differential equation describing conservative and nonconservative changes in DO within the river reach, which could be coupled to the hydrodynamics simulated by USTFLO. The development of this oxygen dynamics equation is described in detail in the next section of this report.

The numerical solution of the Saint-Venant equations (by USTFLO) is not exact because the finite difference numerical scheme must incorporate a number of approximations. The river channel is divided into a number of discrete segments (Δx), and continuous time is divided into finite steps (Δt), which

together form a computational grid. This one-dimensional segmented approach requires a number of assumptions about conditions in a river reach. The validity of these assumptions, relative to the river reach below Conowingo Dam, is discussed below.

- Flow is well-mixed vertically. For the river reach between Conowingo Dam and the fall line, measurements of DO and temperature mixing of the discharge water under different discharge volumes show that this assumption is valid for all conditions.

- The channel is sufficiently straight and uniform in the reach so that the flow characteristics can be physically represented by a one-dimensional model. This assumption is valid during periods of dam discharge, when the flow spreads across a large portion of the river bed and moves straight downstream. However, under shutdown conditions, most of the flow is confined to a channel meandering down the river bed, and consists primarily of dam leakage and slow drainage of the tailrace pool. Simulation using USTFLO can accurately simulate the transport of water through a whole cross section. However, the confinement of flow to one or a few channels means that there are large variations in local flow which the model cannot simulate. At a discharge of 4000 cfs, flow appears to spread over most of the riverbed (Photo Science 1980) and distinct flow channels are no longer visible. Thus, the one dimensional flow assumption appears valid for discharges as low as 4000 cfs. Below this discharge, the model can only be used to simulate average flow in a cross-section. A two-dimensional model is probably needed for the drainage and leakage flow during shutdown periods, or for discharges below 4000 cfs. However, available data are not sufficient to calibrate a two-dimensional model.

- The velocity is the same throughout a cross section. Data collected downstream of Conowingo Dam by the Susquehanna River Basin Commission (SRBC)(Jackson and Lazorchick 1980) show large variations in velocity across a cross section at a number of discharge levels, apparently related to the very rough topography of the river bottom. However, it is not feasible to increase model dimensionality or segmentation to simulate these microscale variations in velocity (e.g., to simulate two or three flow dimensions, with segment lengths on the order of a few feet). Thus, simulations with USTFLO characterize average conditions in a segment,

not conditions at any point. At discharges of 4000 cfs or larger, flow spreads across the riverbed, and microscale velocity variations do not affect the simulation of water transport. At discharges below 4000 cfs, the model is able to only simulate the average velocity on a cross-section.

- The water surface across the channel is horizontal. Although differences in cross-channel water height of up to 1 ft have been observed at discharges less than 15,000 cfs, they appear to be related to water backing up behind local topographic features (e.g., rock ledges) that become completely submerged at discharges above 15,000 cfs. Again, these effects probably cannot be simulated with any feasible level of modeling detail. However, such buildup areas are not likely to affect model results, so long as measurements of water surface elevation used in calibrating the model were taken from free flowing areas (which was the case for data used in the present study).

- The slope of the channel bottom is small. Although large local bottom slopes exist, structuring the model with sufficiently large segments will eliminate the effects of such irregularities, since the average slope of the river bottom between the dam and the fall line is ~ 1/1000. Thus, the assumption appears valid for the long segments used in the present study.

- Hydrostatic pressure prevails at every point in the channel. This assumption is violated in the vicinity of the turbine discharge boils, where large elevations in water surface are controlled by the dynamics of water flowing from the the reservoir, not by the hydrostatic pressure of the river. For this reason, the upstream boundary we chose for the model is 300 ft downstream of the turbine discharge boils, where normal, free-flowing surface elevations always occur.

- Manning coefficients for steady state are applicable to unsteady flow. Although the coefficients are likely to change with discharge (i.e., the effect of bottom friction probably decreases as the depth of overlying water increases), we assumed that the coefficient value at a given flow was not affected by any preceding changes in flow. We evaluated this assumption in simulations by comparing simulated vs observed water -surface elevations during changes in discharge, and observed no major deviations.

Choice of River Segmentation

USTFLO approximates the differentials of the Saint-Venant equations using discrete differences between adjacent points on the x-t grid in the numerical solution. It then uses an explicit scheme, which expresses the unknowns in the finite difference equations as functions of known quantities and solves them directly. However, in such an explicit numerical scheme, the choice of segment length and time-step for the numerical solution is constrained by the Courant numerical stability criterion (Yen 1979):

$$\Delta t < \frac{\Delta x}{C} = \frac{\Delta x}{(\sqrt{gz} + U)} \qquad \text{(Eq.3)}$$

where Δx is the river segment length, Δt is the time step, C is the phase speed of a small-amplitude gravity wave, z is the average water depth along Δx, and the other terms are as previously defined. To simulate longitudinal variations of DO within the river, we first needed to calculate the hydrodynamic unknowns (e.g., water velocity, height) at a number of locations along the river reach between Conowingo Dam and the fall line, 17,060 ft downstream (Fig. II-1). If Δx is chosen as 2,096 ft, yielding eight segments, then (from Eq. 3) typical flow values (U, z) for the reach lead to time steps on the order of a few minutes or less. To satisfy the Courant stability criterion (Eq. 3) under all flow conditions, we chose a time step (Δt) of one second. Because of the "leapfrog" or centered-difference computation scheme used in its explicit computational method (HEC 1977), the model produces accurate outputs for only five odd-numbered transects of the nine that bound the segments (Fig. II-1). Thus, the model only simulates independent outputs for four points.

To apply USTFLO to the Susquehanna River reach of interest, we specified the geometry of each segment of reach. The inputs used by USTFLO to describe the geometry as a function of discharge are river cross-sectional area vs. water elevation,

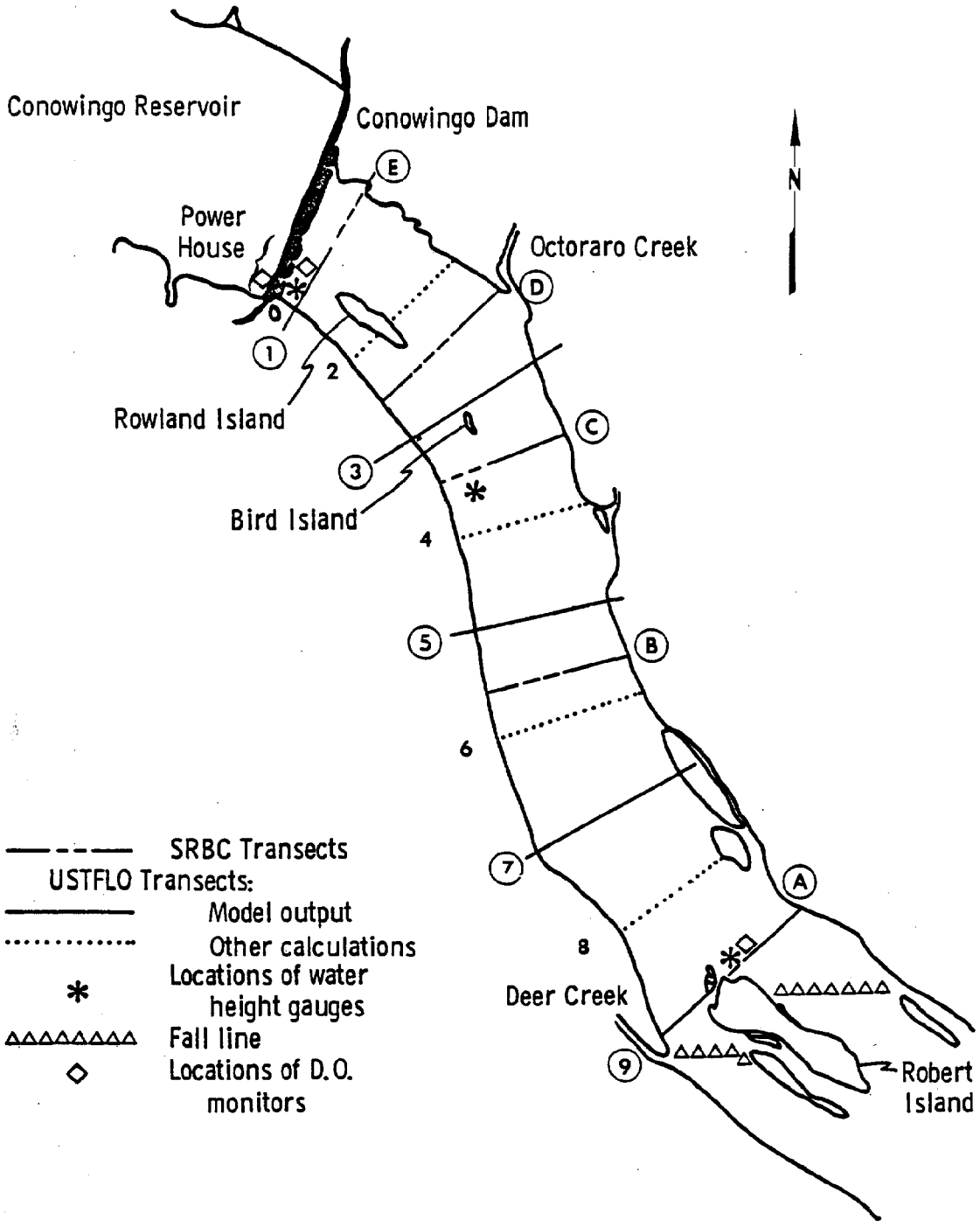

Figure II-1. Susquehanna River between Conowingo Dam and the fall line, showing longitudinal segmentation: letters are transects used in SRBC hydrology studies; odd numbers are downstream boundaries of USTFLO segments at which independent output estimates are simulated; even numbers are other boundaries used in the model's finite difference calculations; asterisks are locations of water height gauges deployed in 1981; diamonds are locations of DO monitors deployed in 1980 and 1981.

wetted perimeters of the cross sections (hydraulic radius), surface widths, and Manning bottom-friction coefficients (Table II-1). This information was derived from data from past hydrology studies in this river reach (Jackson and Lazorchick 1980; Photo Science, 1980).

Initial Conditions

To specify initial conditions, USTFLO needs data on water surface elevations and flows (either velocities, U, or water mass fluxes, Q) at each of the eight segments at time, t = 0. Since data from most rivers are not usually as complete as those used here, USTFLO was designed to accept inaccurate field measurements as initial conditions (which can be rough approximations). The model then recalculates the exact hydraulic conditions needed to satisfy the requirements of the integration scheme (i.e., to prevent unwanted numerical transients from hiding the real hydraulic transients of interest). We encountered a difficulty in attempting to use accurate measurements of water surface elevations and discharges (made during aerial surveys of this Susquehanna river reach) as initial conditions in USTFLO simulations. The initial conditions for water elevations calculated by USTFLO differed from the presumably accurate field measurements that had originally been specified. To correct this, we modified the Manning bottom friction coefficients in the eight segments until differences between the observed and calculated water heights were reduced to less than 0.5 ft. This discrepancy was judged negligible given the variability inherent in estimating water heights across a cross-section (Jackson and Lazorchick 1980).

Boundary Conditions

The specification of boundary conditions for USTFLO is somewhat complex. For this Susquehanna River reach, the model

Table II-1. Geometric parameters for 5 model transects at different water elevations

Transect	Elevation (ft, MSL)	Cross-Sectional Area (ft^2)	$R^{2/3}$ (Hydraulic Radius)$^{2/3}$	Water Surface Width (ft)	Manning's n
9	0.00	453	0.60	314	0.090
	1.00	1850	1.00	1083	0.090
	2.00	4785	1.27	1608	0.090
	3.00	8212	1.77	1860	0.075
	4.00	11717	2.23	2215	0.060
	5.00	15250	2.64	2703	0.050
	6.00	18809	3.03	3099	0.040
	7.00	22392	3.38	3274	0.030
	8.00	25998	3.73	3302	0.030
	9.00	29607	4.07	3304	0.030
	10.00	33216	4.39	3304	0.030
	11.00	36825	4.70	3304	0.030
	12.00	40434	5.01	3304	0.030
	13.00	44043	5.30	3304	0.030
	14.00	47652	5.58	3304	0.030
	15.00	51261	5.86	3304	0.030
	16.00	54870	6.14	3304	0.030
	17.00	58479	6.40	3304	0.030
	18.00	62088	6.66	3304	0.030
	19.00	65697	6.92	3304	0.030
	20.00	69306	7.17	3304	0.030
7	1.24	159	0.21	279	0.090
	2.24	648	0.35	964	0.090
	3.24	1676	0.45	1433	0.090
	4.24	2921	0.98	1669	0.090
	5.24	4434	1.27	2020	0.090
	6.24	6569	1.57	2510	0.075
	7.24	9334	1.91	2937	0.060
	8.24	12483	2.35	3170	0.050
	9.24	15690	2.77	3237	0.040
	10.24	18903	3.16	3252	0.030
	11.24	22117	3.53	3255	0.030
	12.24	25330	3.88	3257	0.030
	13.24	28543	4.22	3257	0.030
	14.24	31756	4.54	3258	0.030
	15.24	34969	4.85	3258	0.030
	16.24	38182	5.14	3258	0.030
	17.24	41396	5.44	3258	0.030
	18.24	44609	5.72	3258	0.030
	19.24	47822	5.99	3258	0.030
	20.24	51035	6.26	3258	0.030
	21.24	54248	6.53	3258	0.030

Table II-1. Continued

Transect	Elevation (ft, MSL)	Cross-Sectional Area (ft^2)	$R^{2/3}$ (Hydraulic Radius)$^{2/3}$	Water Surface Width (ft)	Manning's n
5	2.47	0.0	0.00	52.0	0.090
	3.47	0.0	0.00	173.0	0.090
	4.47	0.0	0.01	269.0	0.090
	5.47	43.0	0.34	394.0	0.090
	6.47	310.0	0.45	710.0	0.090
	7.47	1165.0	0.84	1197.0	0.090
	8.47	2673.0	1.03	1812.0	0.090
	9.47	4947.0	1.41	2420.0	0.075
	10.47	7710.0	1.88	2755.0	0.060
	11.47	10593.0	2.34	2868.0	0.050
	12.47	13490.0	2.76	2917.0	0.040
	13.47	16392.0	3.14	2938.0	0.030
	14.47	19299.0	3.51	2943.0	0.030
	15.47	22207.0	3.86	2943.0	0.030
	16.47	25115.0	4.19	2944.0	0.030
	17.47	28023.0	4.51	2944.0	0.030
	18.47	30932.0	4.82	2944.0	0.030
	19.47	33840.0	5.12	2944.0	0.030
	20.47	36748.0	5.41	2944.0	0.030
	21.47	39656.0	5.69	2944.0	0.030
	22.47	42564.0	5.97	2944.0	0.030
3	3.71	0.0	0.00	47.0	0.090
	4.71	0.0	0.00	53.0	0.090
	5.71	0.0	0.00	65.0	0.090
	6.71	2.0	0.16	114.0	0.090
	7.71	29.0	0.38	248.0	0.090
	8.71	105.0	0.86	466.0	0.090
	9.71	303.0	1.02	838.0	0.090
	10.71	1060.0	1.27	1316.0	0.090
	11.71	2440.0	1.34	1764.0	0.090
	12.71	4429.0	1.48	2197.0	0.075
	13.71	7039.0	1.80	2552.0	0.065
	14.71	10039.0	2.24	2700.0	0.060
	15.71	13073.0	2.67	2713.0	0.050
	16.71	16109.0	3.06	2714.0	0.040
	17.71	19146.0	3.43	2715.0	0.030
	18.71	22185.0	3.79	2716.0	0.030
	19.71	25224.0	4.12	2716.0	0.030
	20.71	28264.0	4.44	2716.0	0.030
	21.71	31304.0	4.75	2716.0	0.030
	22.71	34344.0	5.06	2716.0	0.030
	23.71	37384.0	5.35	2716.0	0.030

Table II-1. Continued

Transect	Elevation (ft, MSL)	Cross-Sectional Area (ft^2)	$R^{2/3}$ (Hydraulic Radius)$^{2/3}$	Water Surface Width (ft)	Manning's n
1	4.94	867.0	1.86	171.0	0.090
	5.94	1230.0	2.17	193.0	0.090
	6.94	1638.0	2.44	216.0	0.090
	7.94	2090.0	2.69	254.0	0.090
	8.94	2597.0	2.85	314.0	0.090
	9.94	3172.0	2.93	393.0	0.090
	10.94	3871.0	3.08	459.0	0.090
	11.94	4595.0	3.40	511.0	0.090
	12.94	5335.0	3.72	775.0	0.090
	13.94	6077.0	4.06	1309.0	0.075
	14.94	6818.0	4.39	1804.0	0.065
	15.94	7560.0	5.00	2025.0	0.050
	17.94	9044.0	5.29	2026.0	0.040
	18.94	10528.0	5.86	2029.0	0.030
	20.94	11270.0	6.13	2029.0	0.030
	21.94	12012.0	6.40	2029.0	0.030
	22.94	12754.0	6.66	2029.0	0.030
	23.94	13496.0	6.91	2029.0	0.030
	24.94	14237.0	7.17	2029.0	0.030

requires the provision of the time variations of discharge, velocity, or water elevations, both at the upper boundary (in the tailrace below Conowingo Dam) and the downstream boundary near the fall line. Any one of the following pairs of boundary conditions are acceptable for this application (HEC 1977):

Upstream	Downstream
• discharge hydrograph (time series of flows)	stage-discharge rating curve
• discharge hydrograph (time series of flows)	stage hydrograph (time series of water heights)
• stage hydrograph	discharge hydrograph
• stage hydrograph	stage-discharge rating curve

At the upstream boundary, we have a continuous time-series hydrograph [available from the US Geological Survey's (USGS) water height gauge in Conowingo Dam] and a discharge hydrograph derived from the stage hydrograph and stage-discharge rating curve (Fig. II-2; Myron Lys, USGS, personal communication). For the downstream boundary condition, we used a stage-discharge rating curve derived by SRBC (Jackson and Lazorchick 1980) at a transect 100 m upstream of the fall line (transect A, Fig. II-1), which can be used for discharges of 12,000 cfs or less. In addition, data from a continuous water height recorder (Potera et al. 1982) were used to extend the SRBC stage-discharge rating to cover the full range of dam discharges (0 - 85,000 cfs).

C. CALIBRATION OF USTFLO TO OBSERVED FLOW DATA

After we completed the specification of model geometry and input data needed to simulate the river reach below Conowingo Dam, our next step was to calibrate the model so that its output closely fitted segments of hydrologic data. We carried out this tuning of model parameters in two stages. First, we calibrated the model to fit detailed field elevations over

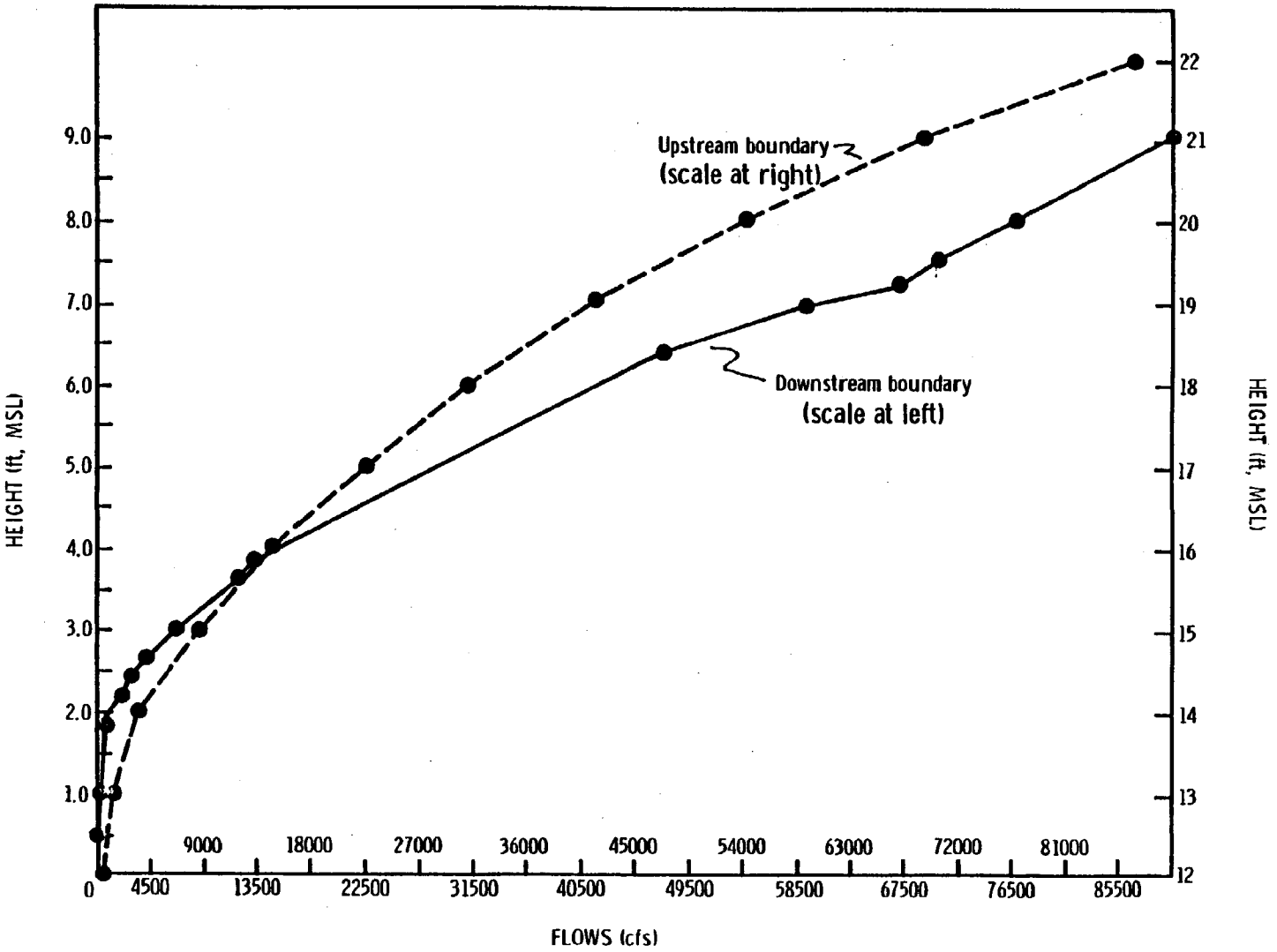

Figure II-2. Stage-discharge rating curves used by USTFLO. Upstream boundary -- U.S. Geological Survey gauge in the dam (dashed line and right-hand water height scale); downstream boundary -- derived from water height gauge data from fall line (solid line and left-hand water height scale).

the entire reach taken at three steady-state discharges (Photo Science 1980). Next, we fitted water surface elevations to time-series measurements made under unsteady discharge conditions, but at only two locations along the river reach. Photo Science's (1980) aerial survey measured water surface elevations over the river reach at three steady-state flows:

- ~ 900 cfs,
- ~ 4,000 cfs
- ~ 12,000 cfs.

Water surface elevations were estimated from the air and ground simultaneously (by Photo Science and SRBC, respectively) at transects A-E (Fig. II-1). These SRBC transects do not coincide with the transects where USTFLO estimates hydraulic parameters (transects 3, 5, 7, and 9; Fig. II-1) because USTFLO requires even segment spacing. However, it is still possible to compare observed and simulated water elevations (Fig.II-3).

For boundary conditions in the steady-state simulations, we used the discharge hydrograph from Conowingo Dam (upstream) and a stage-discharge rating curve derived from SRBC measurements at transect A (downstream). We adjusted Manning bottom friction coefficients so that simulated water elevations agreed (± 0.25 ft) with observed elevations at SRBC transects A-D. However, larger differences between observed and simulated data are evident at model transects 3, 5, and 7 (Fig. II-3). These are probably due to the irregular bottom topography of the river reach, including features such as two rock outcrops across the channel (Photo Science 1980). Such details cannot be included in USTFLO since surveyed bottom topography data are limited to the five SRBC transects. The spatial resolution of the model could be improved only if data were taken at a number of additional cross-sections. In summary, under steady-state conditions, USTFLO simulates a reasonable fit to field data, and probably cannot be further improved with data presently available.

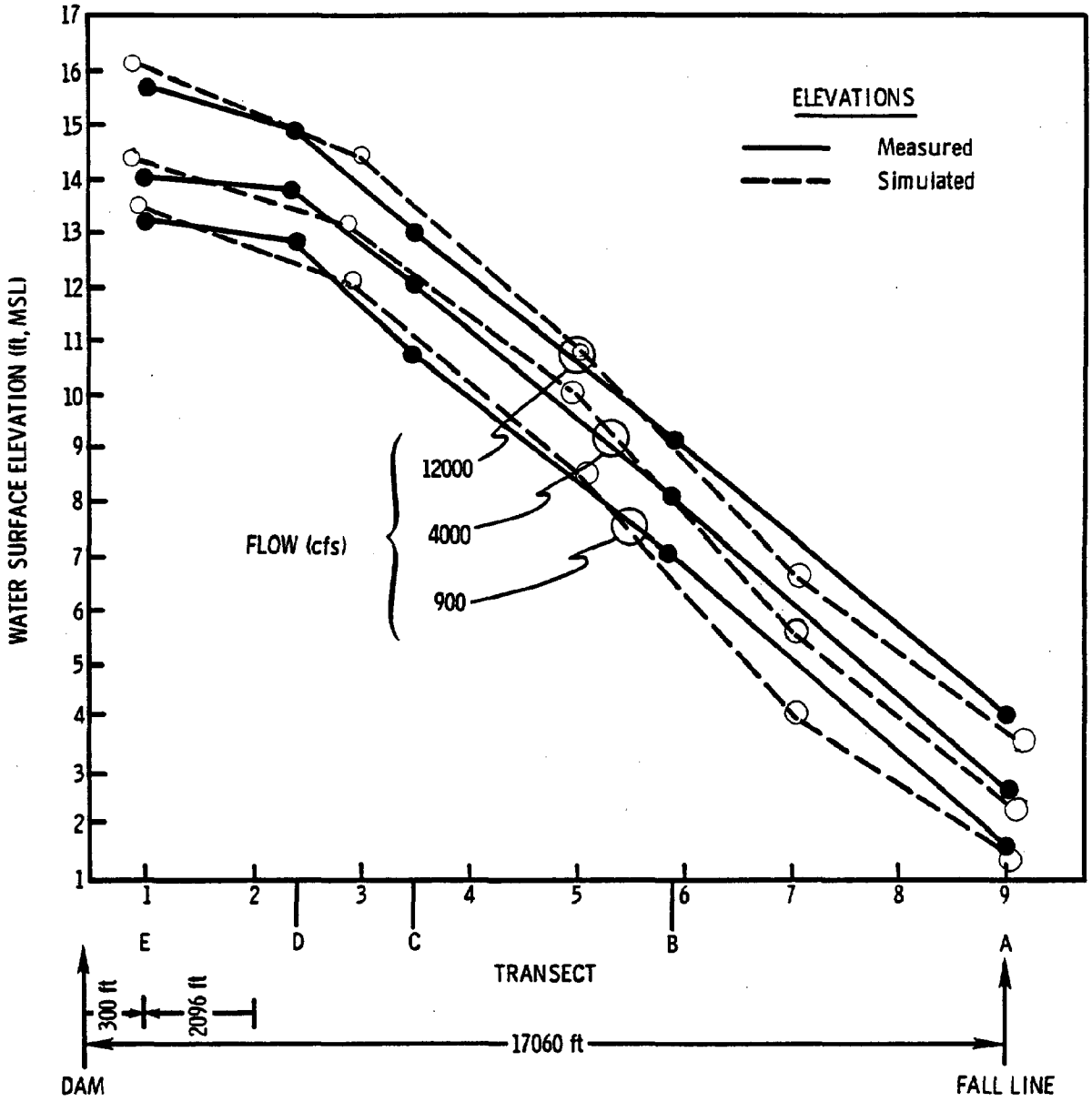

Figure II-3. Measured and simulated water surface elevations along the river reach for three steady-state flows. Solid lines: water surface elevations measured by SRBC at Transects A-E, and by Photo Science (1980) along entire river reach. Dashed lines: water surface elevations simulated by USTFLO at Transects 3, 5, 7, and 9.

For calibration of the model with unsteady flows, we used data from 1981 when continuous water height gauges were deployed near SRBC transects C and A (Fig. II-1). The stage-discharge rating curve at transect A, which we used as the downstream boundary condition for USTFLO, was derived by SRBC using data collected during flows less than 12,000 cfs. To simulate unsteady conditions, we had to derive a new rating curve that included data for the higher flows characteristic of normal operating discharges by the dam. Accordingly, we prepared a new composite rating curve using height data from the gauge at transect A on 27-28 June and measured dam discharges at the same time, plus the stage-discharge data from Photo Science's steady-state measurements at the same place (Fig. II-2).

Initial calibration simulations of river stages using the actual dam discharge hydrograph from 27-28 June indicated that the model overestimated water heights at transect C by about 1 ft at full discharge (Fig. II-4). We suspected that the reason was model overestimation of the effect of bottom friction at high flows. To correct this overestimation, we empirically adjusted the Manning coefficient of each segment so that it decreased as discharge increased (Table II-1). This correction eliminated the discrepancy (not shown) so that simulated heights at transect 3 were not distinguishable from measured data at SRBC transect C (after correcting for the 1.0 ft water height difference due to the 1200 ft longitudinal distance between the two transects).

D. VALIDATION OF USTFLO

We validated the calibrated hydrodynamics of USTFLO using data from a separate time period in 1981. Figure II-5a shows data for simulated water elevations at model transects 1, 3, 5, 7, and 9. The correspondences between measured and simulated water elevations at transect 3 (SRBC transect C; Fig. II-5b), and measured and simulated water elevations at transect 9

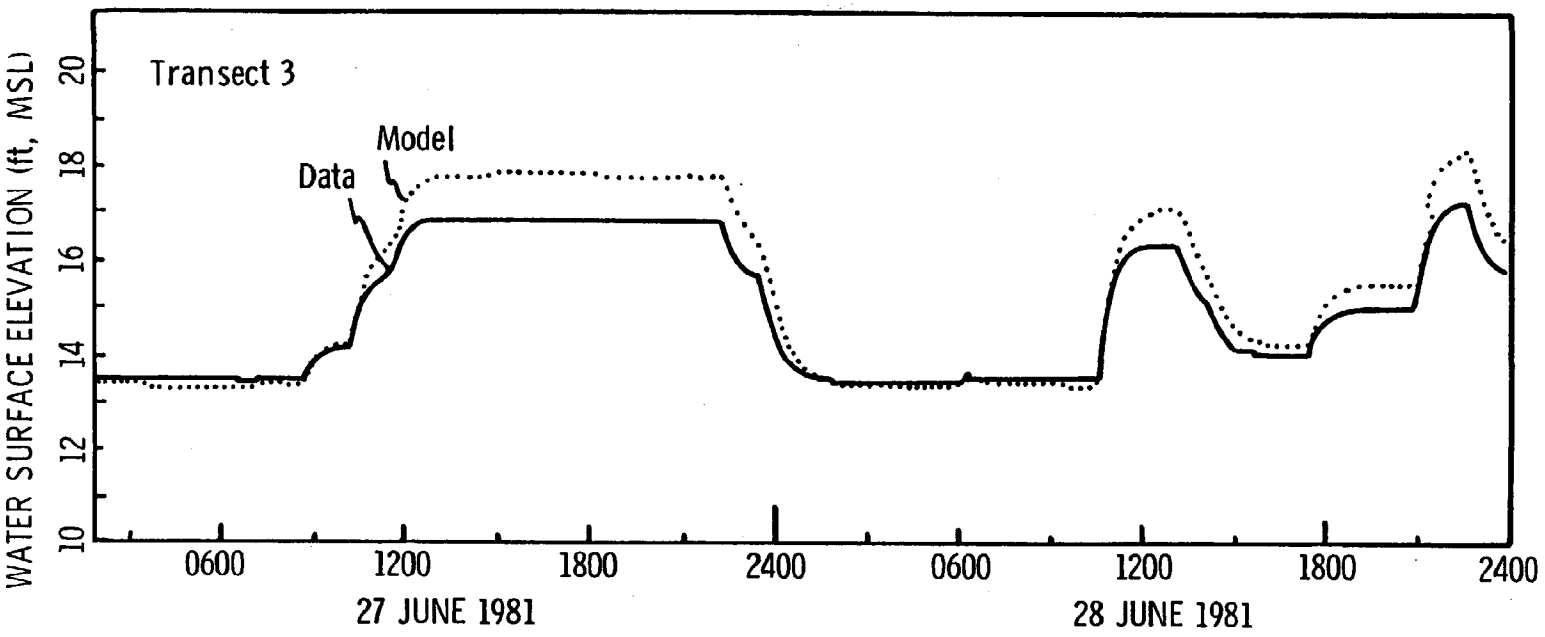

Figure II-4. Initial hydrodynamic calibration run, using constant Manning bottom friction coefficients. Lack of fit (~ 1.0-ft difference) of model to observed data at high discharges was corrected by reducing Manning coefficients as discharge increased. In a subsequent run (not shown), differences between simulated and observed heights were reduced to an average of 0.12 ft (see also Table III-3 and Fig. III-15a).

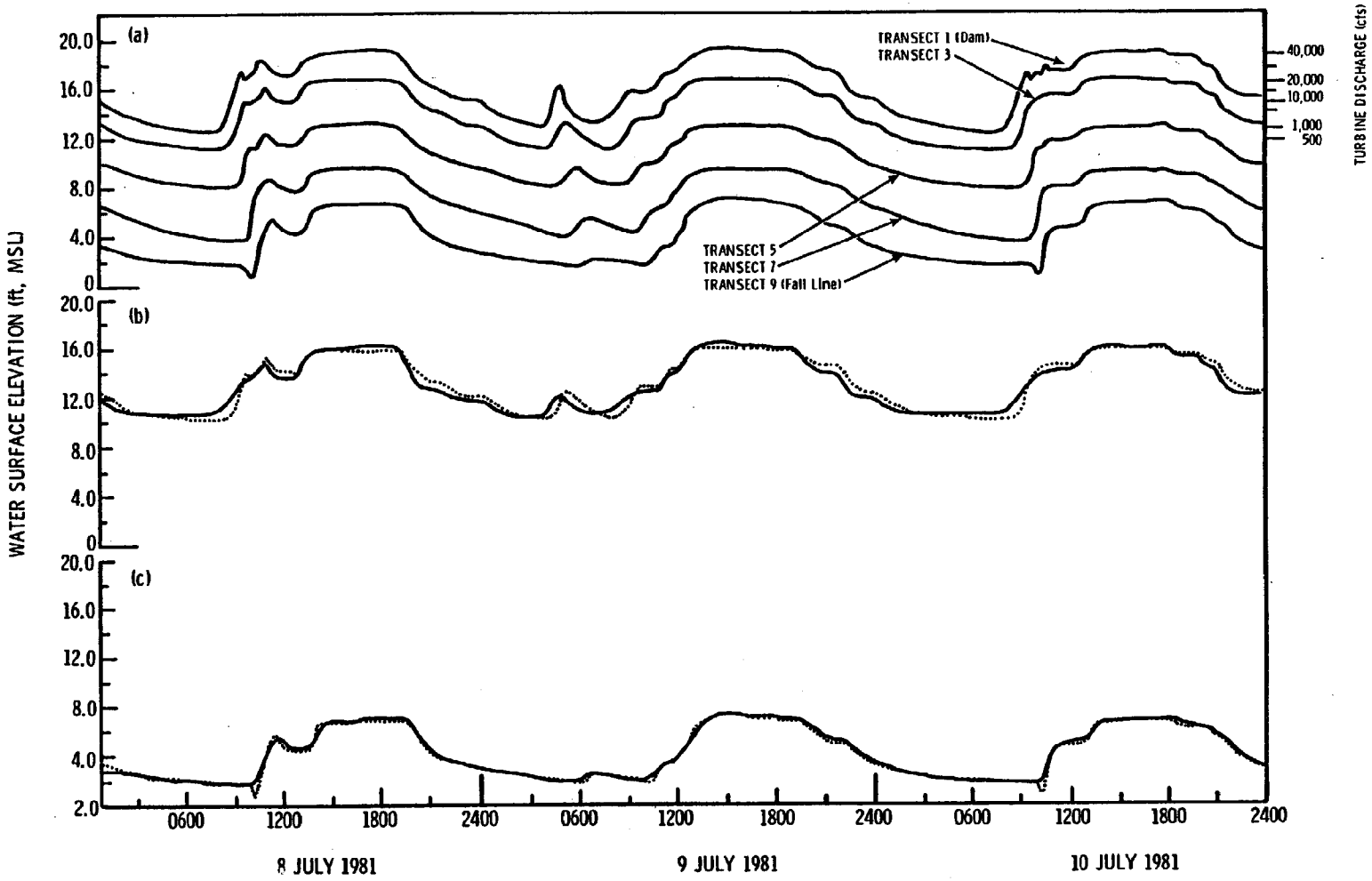

Figure II-5. Validation of hydrodynamic model, 8-10 July 1981. (a) Simulated water surface elevations at five USTFLO transects. Transect 1 is water surface elevation at the dam corresponding to the turbine discharge hydrograph used as a model boundary condition (scale at right). (b) Simulated water surface elevation at transect 3 (solid line), and observed water surface elevation at gauge at transect 3 (dotted line). (c) Simulated (solid line) and observed (dotted line, partially hidden) water surface elevations at transect 9 at the fall line.

(SRBC transect A; Fig. II-5c) show the agreement of the model with real data for fluctuating flows over the period 8-10 July 1981. There is close agreement between measured and simulated water elevations (Figs. II-5b and II-5c). Additionally, the correspondences between simulated water elevations (Fig. II-6a) and simulated velocities at the same transects (Fig. II-6b), over a wide range of discharges, confirms the ability of the calibrated model to simulate water transport from conditions of turbine shutdown up to full turbine discharge--approximately 85,000 cfs. Flows above 85,000 cfs occur only when the dam passes water through the spillways. Under these conditions, it is difficult to make the field measurements needed to extend the calibrated range of the model.

As stated earlier, a validated hydrodynamic model is a prerequisite for any simulation of conservative transport of a substance by river flow. This is also true for the simulation of oxygen, a nonconservative substance which is affected by both conservative transport and in situ physical and biochemical processes. Since the hydrodynamic model has been validated sufficiently and the physical processes embodied in the model are essentially invariant, we will not present any further hydrodynamic validation data during the following discussion of DO simulations.

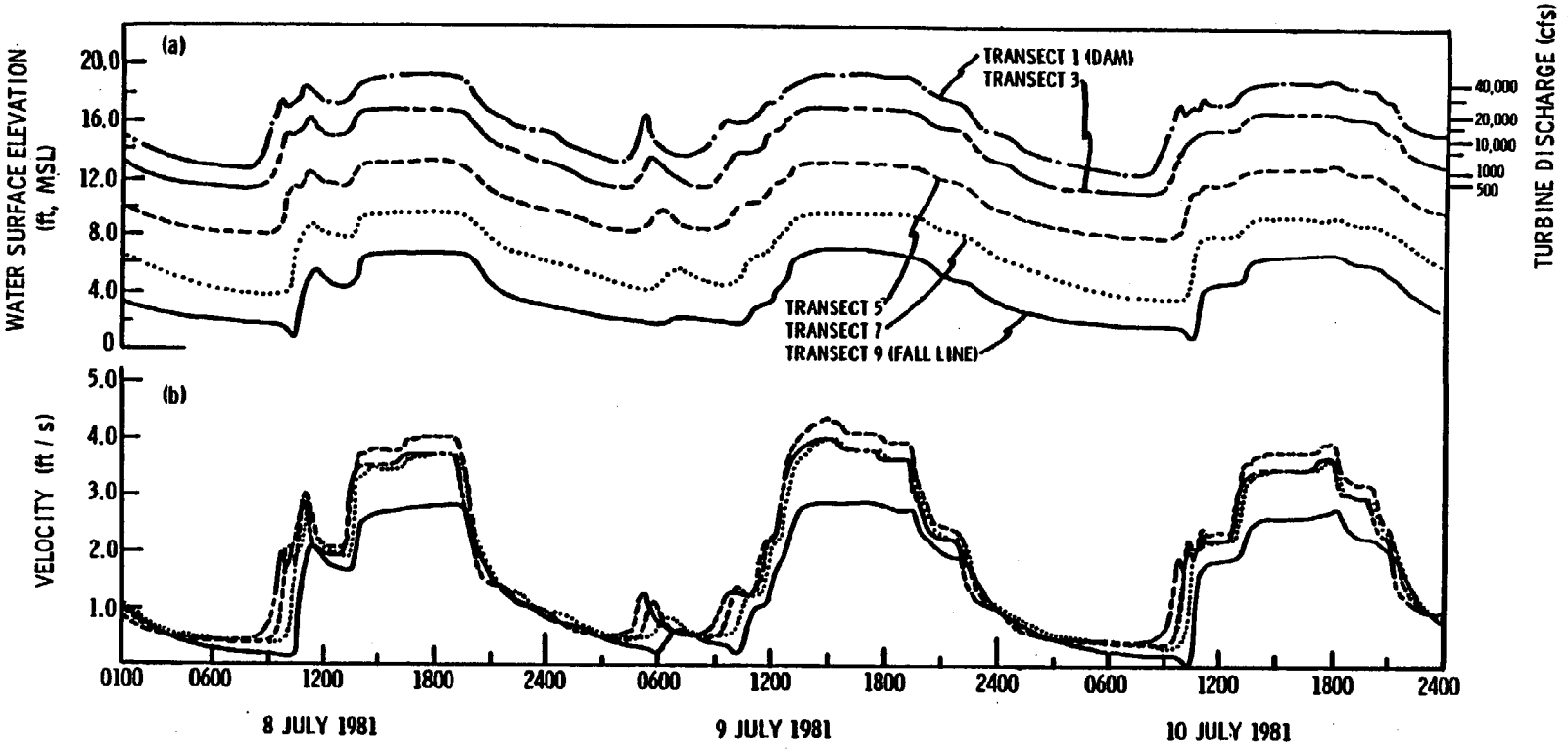

Figure II-6. Validation of hydrodynamic model, 8-10 July 1981. (a) Simulated water surface elevations at five USTFLO transects. Transect 1 is water surface elevation at the dam corresponding to the turbine discharge hydrograph used as a model boundary condition (scale at right). (b) Simulated average velocities at transects 3, 5, 7, and 9. Correspondences between water surface elevation and velocity at each transect confirm that peaks in elevations are in phase with increased velocity and water transport.

III. MODEL OF DISSOLVED OXYGEN DYNAMICS

A. BACKGROUND

In the previous section, we described the calibration and validation of USTFLO. This hydrodynamic model can now serve as the basis for a model of the conservative transport of any substance passively carried by water flow. However, a mass-balance simulation of a material whose concentration is modified by in situ biological or chemical processes, such as dissolved oxygen (DO), requires the quantification of a number of physical and biochemical processes affecting it within the river reach.

The widespread problem of DO depletion in rivers has been under study for decades. The classic model of Streeter and Phelps (1925) described changes in DO with time in terms of two phenomena: oxygen depletion in water due to bacterial decomposition of organic matter (BOD), and reaeration due to oxygen diffusion from the atmosphere. This BOD-based model has undergone many modifications and improvements over the years (Krenkel and Novotny, 1980). However, we chose an alternative approach to simulate DO, in which we estimate the production and respiration of oxygen by more components than are accounted for in the BOD model. The model described in this report performs a mass-balance calculation for DO, based on estimates of the rates of gross production and respiration of the water-column community (including phytoplankton, zooplankton, and bacterial metabolism, as well as purely chemical oxidation) and the benthic community (i.e., epiphytic algae, bacteria, and invertebrates). We also consider atmospheric reaeration and nekton (fish) respiration.

B. DIFFERENTIAL EQUATION DESCRIBING OXYGEN RATE OF CHANGE

Within any river segment, the rate of change in the mass of dissolved oxygen depends on: the mass flux of oxygen into

the segment through its upstream boundary; the flux out of the segment through its downstream boundary; diffusion of oxygen through the air-water interface; oxygen consumption due to respiration of the water-column, benthic, and nektonic communities; and photosynthetic oxygen production of the water-column and benthic communities. These rate processes are incorporated into the model by the following equation:

$$\frac{d(VC)}{dt} = Q_{in}C_{in} - Q_{out}C + K_2(C^* - C)V + V(-R_{wc} - R_n) + S(P_b - R_b + DP_{wc}) \qquad \text{(Eq. 4)}$$

where

V = volume

C = concentration of dissolved oxygen
t = time

Q = flow

K_2 = reaeration coefficient

C* = saturation of DO

R = respiration

wc denotes water-column community

n denotes nekton

S = surface area

P = gross production

b denotes benthos

DP_{wc} = water-column production integrated over depth

and further:

$$V(t) = V(t-1) + (Q_{in} - Q_{out})t$$

To simulate DO dynamics longitudinally along the river reach, we coupled Eq. 4 to the Q, V, and S terms simulated by USTFLO and integrated it numerically (using a fourth-order Runge-Kutta scheme) for each segment. Numerical stability

was not of concern for the solution of the DO equation, so we chose a Δt of 15 minutes. Actual DO simulations used stored hydrodynamic data from USTFLO runs, which were sampled every 15 minutes. As outputs, the DO model calculates DO values at transects 3, 5, 7, and 9 (Fig. II-1) every 15 minutes.

This DO model configuration is based on several assumptions. First, all oxygen passing into a given river segment is assumed to be mixed instantaneously. Next, DO within any segment is assumed to be relatively homogeneous, so that the average DO simulated by the model is representative of actual DO concentrations anywhere in the segment. This assumption probably is not met in the field during turbine shutdowns and very low discharges when DO values in isolated pools tend to diverge from this average, and from one another (Philipp and Klose 1981). This inherent variability in the system means that the model cannot predict DO at any single point, even though the simulated DO value for a segment is expected to agree with the average of a large number of individual measurements in the segment. There are insufficient data both on the hydrodynamics and on DO distributions to permit refinements in the spatial resolution in the model so that the variability can be simulated.

Another assumption is that the DO of the turbine discharge is the same as the DO crossing the upstream boundary of the model (located 300 ft downstream of the dam, for reasons already discussed). In other words, we assume that DO does not change (e.g., due to reaeration) in the 300 ft stretch. At present, there is much uncertainty about the accuracy of DO measurements in the turbines, so there is no way to quantify any such change using available data. However, it is possible to make some first order judgements of the importance of this effect based on the fit of the model to DO data in the upstream model segments, as we shall do later.

Also inherent in the DO model is the assumption that longitudinal dispersion of a transported substance in the river reach is small compared to its advective transport (i.e., a concentrated plug of material does not spread longitudinally as it travels

downstream). An explicit dispersion term is not employed in the model, but the explicit integration scheme does generate an implicit numerical dispersion. To determine whether this numerical dispersion approximates the actual dispersion of a substance being transported in the river reach, we calculated actual dispersion from observations of pulses of dye released at different discharge rates, and numerical dispersion from simulations of the same dye-release events.

Dispersion will cause a discrete pulse of dye introduced at the upstream end of a river reach to spread longitudinally as it travels downstream -- the leading edge of the dye mass will travel faster than the trailing edge. A concentration-vs-time curve measured at some downstream point will show a peak at the average travel time of the dye, and will typically exhibit a normal distribution about the peak. The variance of this distribution directly yields a coefficient of dispersion for the reach (Levenspiel and Smith 1957):

$$D_L = \frac{UL}{8} [(8\ \sigma^2 + 1)^{1/2} - 1] \qquad \text{(Eq. 5)}$$

where

D_L = dispersion coefficient, m^2/s

U = velocity in the reach, m/s

L = distance between the release and measurement points

$\sigma^2 = \left(\frac{Q}{V}\right)^2 \sigma_\theta^2$ = variance of the concentration curve (dimensionless)

Q = flow, m^3/s

V = volume, m^3

σ_θ^2 = statistical variance of the concentration vs time curve.

To measure both the actual time of travel and dispersion in the river reach, a number of dye pulses (Rhodamine WT) were released at the dam during several near-steady discharges

(Potera et al. 1982). Subsequently, time-series concentrations of dye were measured in the flow channel at transect C, and at a number of stations distributed across transect A (both in the main flow channel, and in slower flowing areas). A typical time-concentration curve is shown in Fig. III-1. We calculated variances of these and similar data and substituted them into Eq. 5. The resulting dispersion coefficients are listed in Table III-1a -- values are in the range of 1.26 - 147.0 m^2/s. The majority of these values fall within the range reported by Krenkel and Novotny (1980) of 0.3-30 m^2/s for large rivers. The broad range of values at transect A is probably due in part to real differences in travel times and dispersions of dye masses traveling in the main flow channel rather than along less direct paths in rocky shallows. Thus, the measured dispersion of this river reach appears typical of larger rivers.

While the oxygen model does not include an explicit dispersion term, the instantaneous mixing of incoming water in each segment numerically disperses oxygen along the reach, which can be quantified using Eq. 5 and compared with real dispersion rates. To estimate this implicit dispersion in the model, we simplified Eq. 4 by eliminating all nonconservative terms:

$$\frac{d(VC)}{dt} = Q_{in} C_{in} - Q_{out} C \qquad \text{(Eq. 6)}$$

and ran the simulations with Δt = 15 min and the duration of the initial tracer pulse set at 15 min. Simulated time-concentration curves for four transects for a 3,500 cfs discharge are shown in Fig. III-2. Although the tracer pulse flattens and broadens, D_L values remain relatively constant as the pulse travels downstream (Table III-1b). Simulations were also run with Δt = 5 min, which produced little change in calculated values of D_L at the same flows. Dispersion estimates from the dye data (Table III-1a) and the simulated results (Table III-1b) are similar for all but the 40,000 cfs discharge (which is a high flow even for large rivers, and is outside the range of

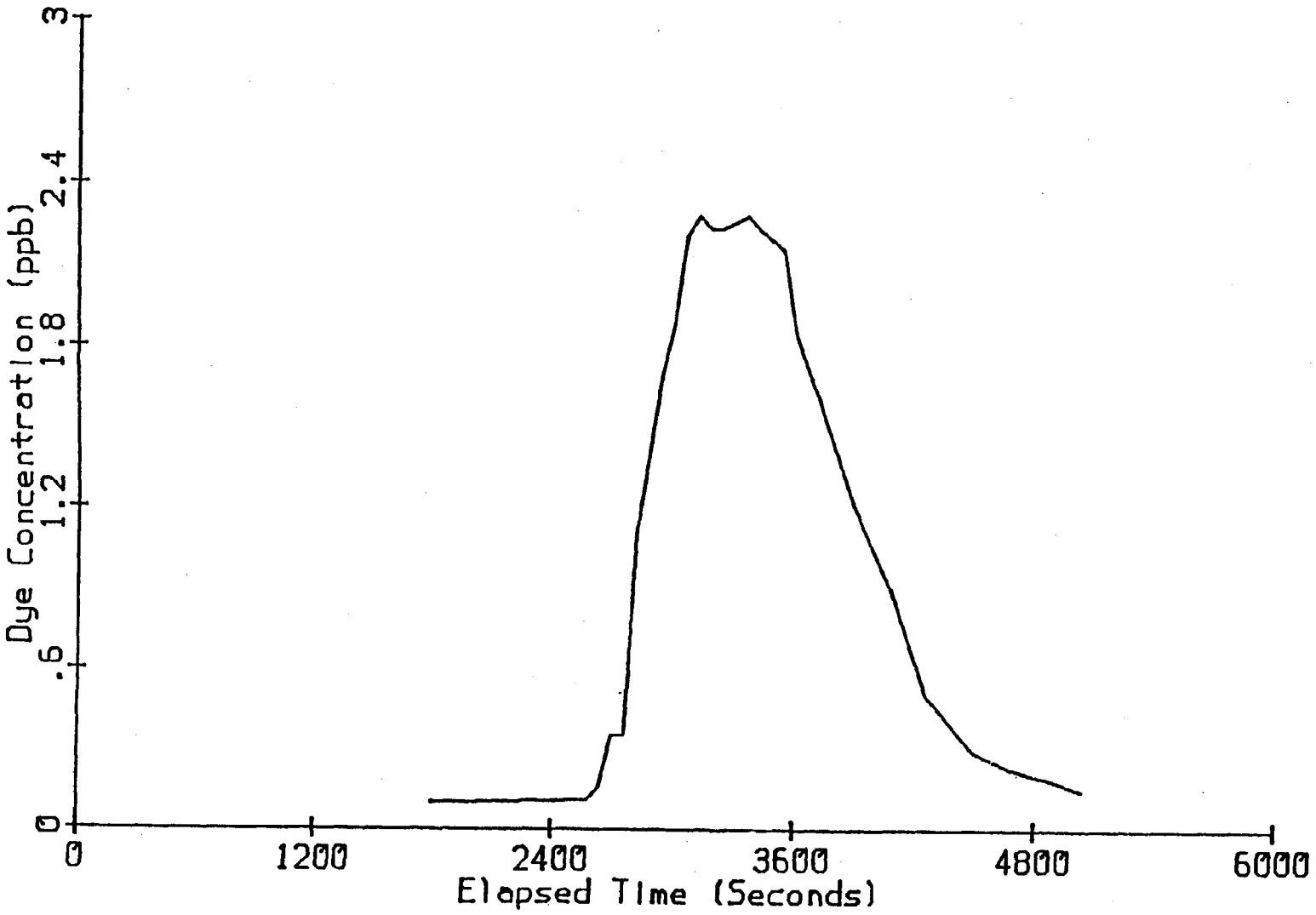

Figure III-1. Typical time-concentration record from a river station during downstream transport of a dye mass released at the dam. Data were taken near the water height gauge on transect C; 6 liters of Rhodamine WT dye was released at the dam during a 5,000-cfs steady-state discharge period.

Table III-1a. River dispersion coefficients (from dye release on 26 August and 2 September 1981)

Flow (cfs)	Transect	D_L (m^2/s)
5,000	A	72.9
	A	115.0
	A	33.0
	A	32.2
	A	48.5
	A	21.9
	A	25.9
	A	17.0
	C	6.83
	C	7.14
8,000	A	1.26
	A	136.0
	C	8.51
	C	4.52
40,000	A	147.0
	A	102.0

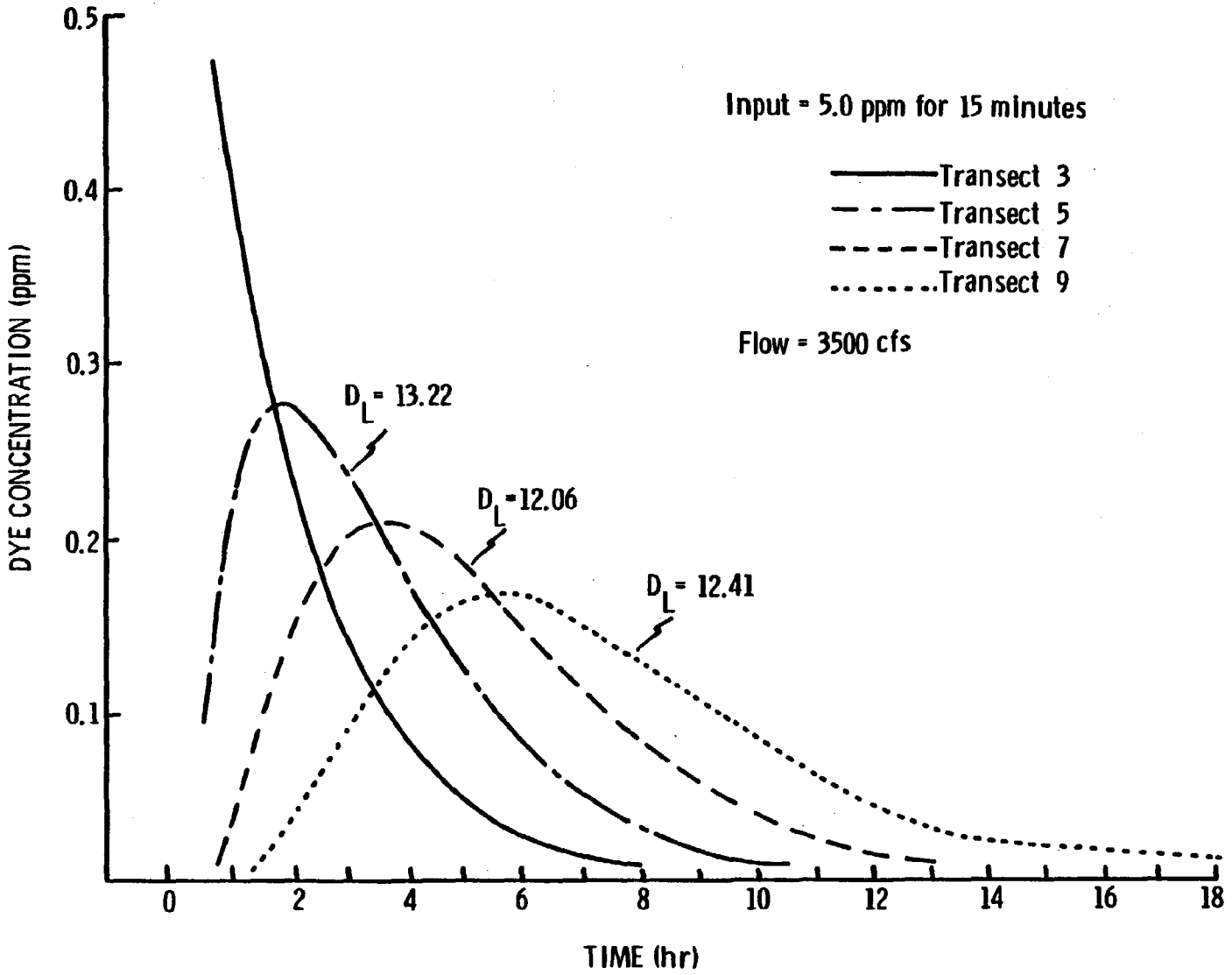

Figure III-2. Simulated time-concentration curves at four downstream transects during a discharge of 3,500 cfs. Curves show effects of implicit numerical dispersion produced by the model as the dye mass moves downstream.

Table III-1b. Model dispersion coefficients (from model simulations at steady-state flows using 2 September 1981 hydrodynamic data)

Flow (cfs)	Transect	D_L (m^2/s) Δt = 15 min	D_L (m^2/s) Δt = 5 min
3,500	3 (~ C)	13.22	
	5 (~ B)	12.06	
	9 (~ A)	12.41	
5,000	3 (~ C)	39.4	34.3
	5 (~ B)	39.9	35.1
	9 (~ A)	36.2	31.5
5,000	3 (~ C)	27.0	50.0
	5 (~ B)	22.4	48.3
	9 (~ A)	21.7	48.3
40,000	3 (~ C)	693.0	604.0
	5 (~ B)	823.0	730.0
	9 (~ A)	895.0	805.0

interest for protecting aquatic habitat). Thus, the model's numerical dispersion is comparable to the actual dispersion of the river reach.

While the dispersive properties accounted for in the model appear similar to those of the real river reach, it is useful to know whether changes in the model's formulation, affecting its dispersive properties, would influence DO concentrations simulated by the model. Accordingly, we made two simulation runs with the complete DO model (Eq. 4, including all the estimated rate coefficients described in detail later) to examine the sensitivity of output DO values to gross changes in numerical dispersion. The first run simulated a segment of time using USTFLO and Eq. 4. In the second run over the same time segment, we modified Eq. 4 so that C (DO concentration of a segment, as a function of time) was set to a constant value within any time step and segment. This was done to simulate water entering each segment during the time step without mixing, (i.e., simulating the downstream transport of discrete plugs of water without intermixing). This artificially eliminated the numerical dispersion inherent in the model. The simulation results showed that oxygen concentrations at transect A in the second run were not detectably different from those in the first, indicating that dispersion had little effect on simulated oxygen values.

To summarize the discussion of dispersion, the numerical dispersion implicit in the model appears to be equivalent to the actual dispersion at low flows in the river reach, as calculated from dye releases. Secondly, simulated DO concentrations show no sensitivity to large changes in this numerical dispersion. Thus, the numerical dispersion due to the nature of the solution scheme satisfactorily simulates the longitudinal dispersion observed in the river reach.

Based on these dispersion analyses, advective processes rather than turbulent dispersion appear to dominate the longitudinal transport of substances dissolved in river water.

This transport mechanism is passive in that the flux of a substance downstream is proportional to the volume of water flowing downstream. This water flow is described by the hydrodynamic equations embodied in USTFLO, so its dynamics also apply to the advective transport of other substances.

While the passive transport of any substance is conservative, the transport of DO is also governed by a number of in situ biological and physical mechanisms that change local DO distributions in the river reach. Below, we consider each of the major sources and sinks of DO in the river reach (Eq. 4) due to the metabolism of components of local biota, and to diffusion of oxygen across the air-water interface.

C. NONCONSERVATIVE PROCESSES AFFECTING DO IN THE RIVER REACH: ESTIMATION OF RATES FOR INCLUSION IN THE DO MODEL

Diffusion

Diffusion of oxygen through the water surface can be described by the following equation:

$$\frac{dC}{dt} = K_2 (C^* - C) \qquad \text{(Eq. 7)}$$

where the terms are defined as in Eq. 4. The rate of change in local DO is determined by two terms: a reaeration coefficient K_2, which is determined by local turbulent mixing, and a DO saturation deficit describing the concentration gradient between the water and air. This process is also commonly called atmospheric reaeration. Since water may become supersaturated with oxygen at times, the term (C* - C) can be negative, indicating a potential loss of oxygen to the atmosphere.

For the present model, we calculated the saturated concentration of DO in each model segment at each time step from the equation of Kester (1975; Eq. A.1 in Appendix A), assuming a salinity of 0.0 and using estimated segment temperatures in the river reach. We simulated the downstream increase in water temperature under daytime shutdown or low discharge conditions

using a relationship derived from measured upstream-downstream temperature differences as functions of discharge volume and time of day (i.e., intensity of solar heating). The function is a sinusoidal temperature increment over a day, which varies downstream temperatures a maximum of 3°C above the temperature of the discharge water (Eq. B.1 to B.4 in Appendix B).

Estimation of the reaeration coefficient for rivers has been the subject of a great deal of research (reviewed by Bennett and Rathbun 1972). A number of methods for empirical measurement of K_2 have been devised, and two of them were applied to the Susquehanna River in 1980 and 1981. In 1980, reaeration was measured in the tailrace on 10 occasions (between 11 May and 12 November; Philipp and Klose 1981). The disturbed equilibrium technique (Bennett and Rathbun 1972) employed in 1980 used a flexible vinyl wading pool filled with water, which floated in the tailrace under low discharge conditions. The water was deoxygenated with sodium sulfide, and the return to saturation was monitored over time. This method assumes that the vinyl wall can transmit at least some of the turbulent energy of the flowing river, so reaeration values in the pool should be similar to true river values. Calculated reaeration coefficients (K_2) ranged from 2.05 to 13.57 (hr^{-1}).

Measurements in 1981 (Potera et al. 1982) used the floating dome technique (Copeland and Duffer 1964; Roques and Nixon, in preparation; Boynton et al. 1978). For this method, a dome is filled with pure N_2 gas and floated on the surface of the water body being measured. The increase in O_2 concentration in the N_2 atmosphere is monitored over time. This method has the advantage that the true turbulence of the water column governs the diffusive flux of oxygen. However, the dome eliminates wind-induced surface turbulence. The apparatus is also somewhat unstable at high velocities (due to discharges above 20,000 cfs); repeated capsizing of the gear aborted all but three measurements below the dam in 1981. The 1980 and 1981 field measurements of K_2 are plotted in Fig. III-3. Most of

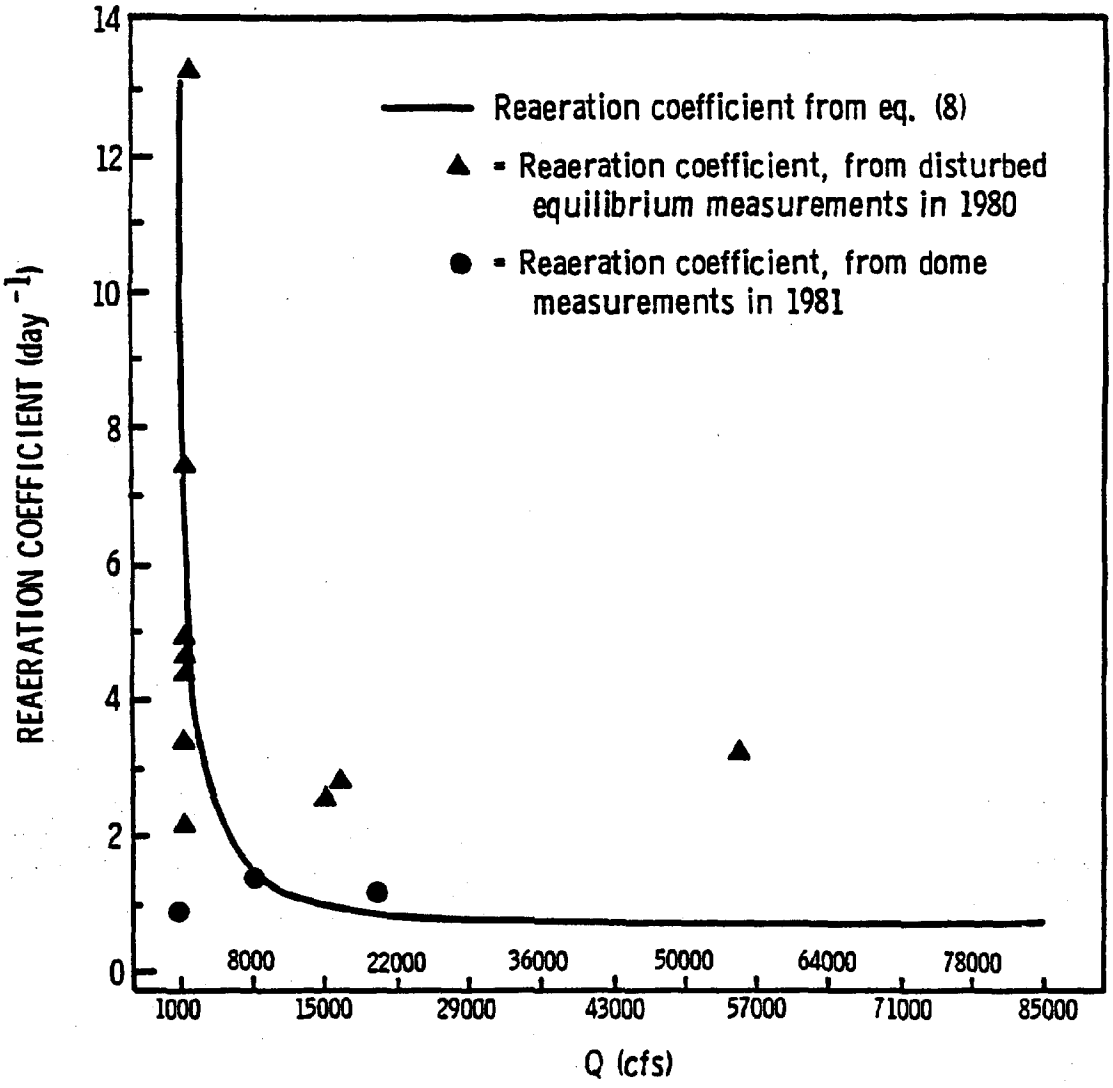

Figure III-3. Reaeration coefficient as a function of discharge.

the data are clustered at low discharges and exhibit a great deal of variation, which prevented a statistical fit to the data. These two methods each suffer some disadvantages. Newer in situ techniques like radiotracer injection would provide accurate estimates at all discharges; however, these methods were not logistically feasible.

To provide an alternate means of estimating reaeration, we reviewed the literature for reaeration coefficient values for other rivers. Bennett and Rathbun (1972) reviewed a number of reaeration studies, each of which proposed an equation to estimate K_2 from depth and velocity. They combined the original data from these studies (over 100 data setes) and estimated a new predictive equation:

$$K_2 = 8.76 \frac{U^{0.607}}{h^{1.689}} \qquad \text{(Eq. 8)}$$

where U is velocity (ft/sec) and h is water depth (ft). Figure III-3 shows a curve of K_2 estimated from this equation, using river-wide averages of depth and velocity at various steady-state discharges from USTFLO simulations. We used Eq. 8 directly to estimate K_2 for each segment of the model.

Nekton Respiration

Fish kills are the major manifestation of DO depletion events, and local concentrations of fish may be major contributors to DO depletion. However, fish are highly mobile within the river reach, and estimates of population numbers and biomass are subject to much uncertainty (Petrimoulx and Klose 1981). Estimates of nekton community respiration, derived from biomass estimates (Philipp and Klose 1981), are even less reliable. Nevertheless, to provide an order-of-magnitude indication of the importance of fish respiration to overall DO dynamics within the river reach, we used the estimate of nekton community respiration in the river reach (Philipp and Klose 1981) derived from estimated biomasses of five major species found there in

1980 (excluding menhaden, whose presence in the area is very unpredictable).

Using estimated river volumes under shutdown conditions, we estimated that the average oxygen consumption by nekton in the reach is 28.14 kg O_2/hr, which is less than 0.01 g O_2/m^3 hr. This value is less than the lowest of any water-column or benthic respiration value measured in the river during 1980. Thus, we feel justified in assuming that this respiration term is usually negligible. Accordingly, its value is set to zero for the simulations presented in this report.

Respiration of the Water-Column Community

Respiration of the water-column community can contribute to the depletion of oxygen. In 1980, a number of measurements of water-column community respiration (as well as production), using the oxygen light-dark bottle technique (Strickland and Parsons 1968; APHA 1975), were made in the study area and in the tidal river reach immediately downstream (Philipp and Klose 1981). Fig. III-4 presents estimates of water-column respiration vs time. The same data are plotted as a function of distance from the dam in Fig. III-5. Variability of these data with respect to time and location of measurement, as well as depth (not shown), is probably due in part to the variation in plankton standing stocks and concentrations of organic matter in the water discharged from the reservoir. Respiration rates increase with increasing temperature (Fig. III-6). Although these data would be expected to follow the exponential Q_{10} relationship, the variability in these data, and/or narrow range of data, prevent a statistical fitting to the exponential model. However, a significant linear relationship (Fig. III-6) exists between temperature and respiration data measured in 1980:

$$R_{WC} = 0.01 + 0.0016\ T \qquad \text{(Eq. 9)}$$

where R_{WC} is water column community respiration (g O_2/m^3-hr) and T is temperature (°C). Statistics for the regression are

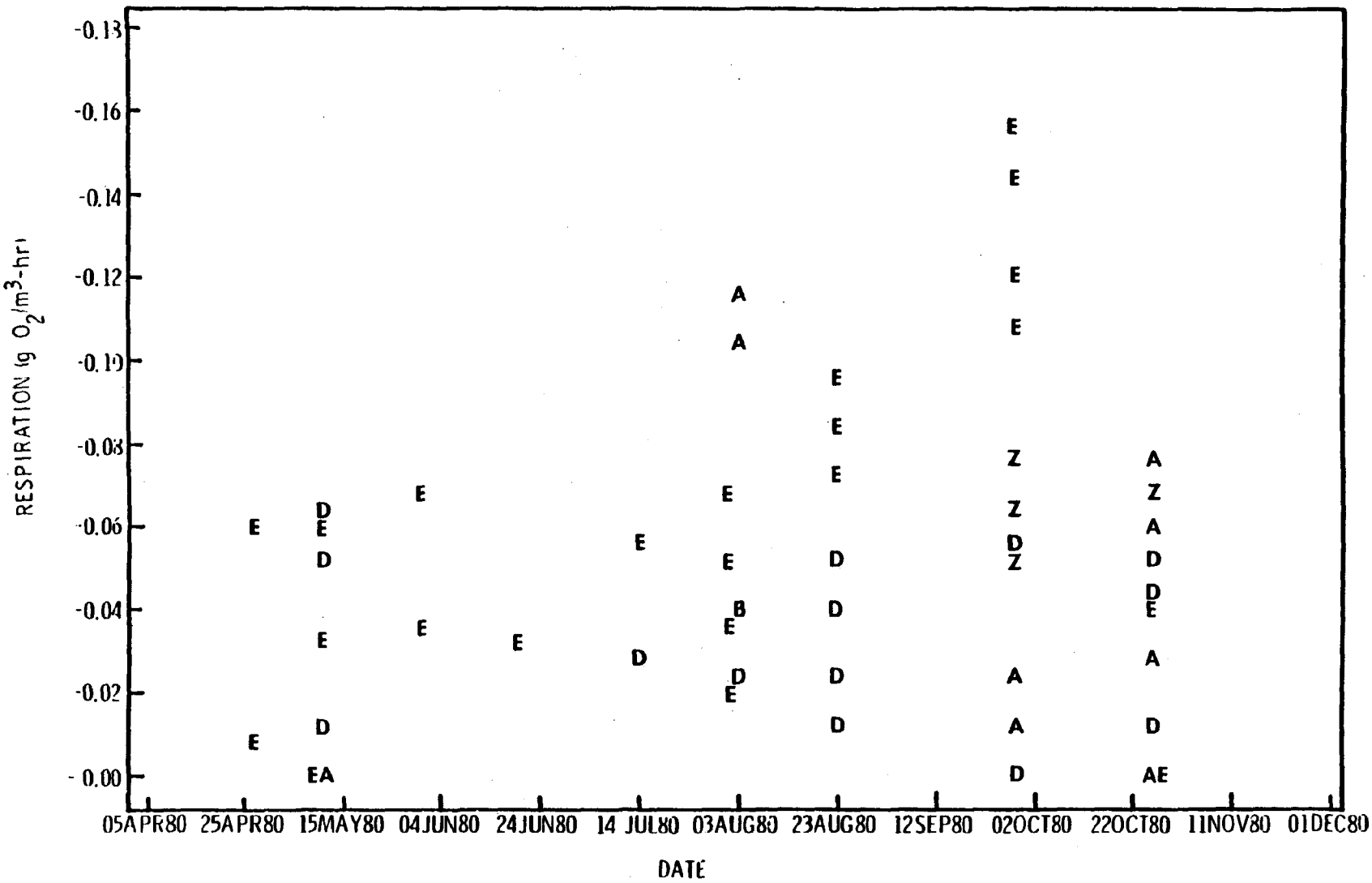

Figure III-4. Estimates of respiration of water-column community, April-October 1980. Data from dark-bottle incubations at SRBC transects (A-E) and at one station in the tidal portion of the river (Z).

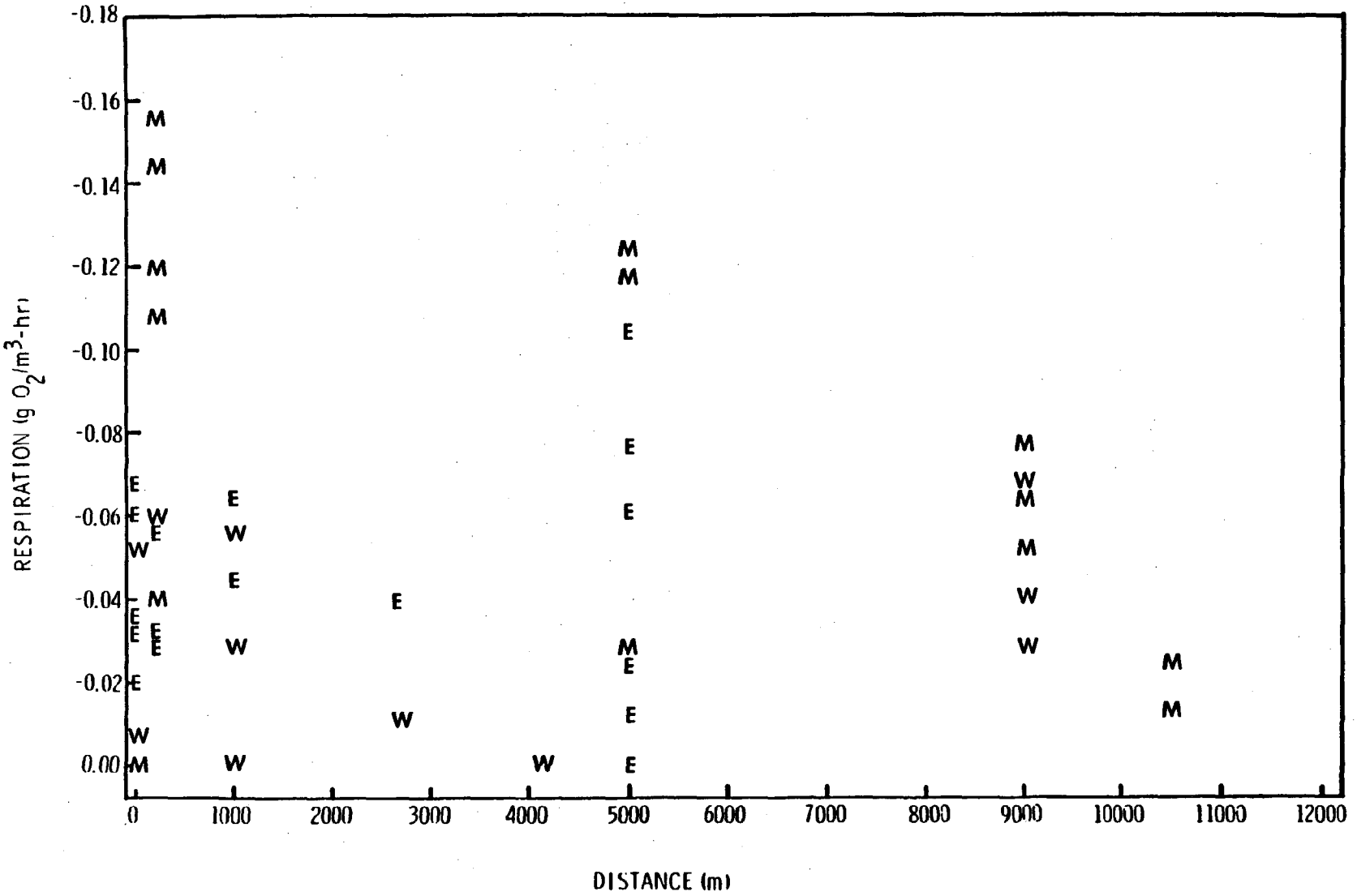

Figure III-5. Estimates of respiration of water-column community vs. distance from Conowingo Dam (meters). (E) Station on east side of river; (M) Station near middle of river; (W) Station on west side of river. Fall line is at 5,200 m.

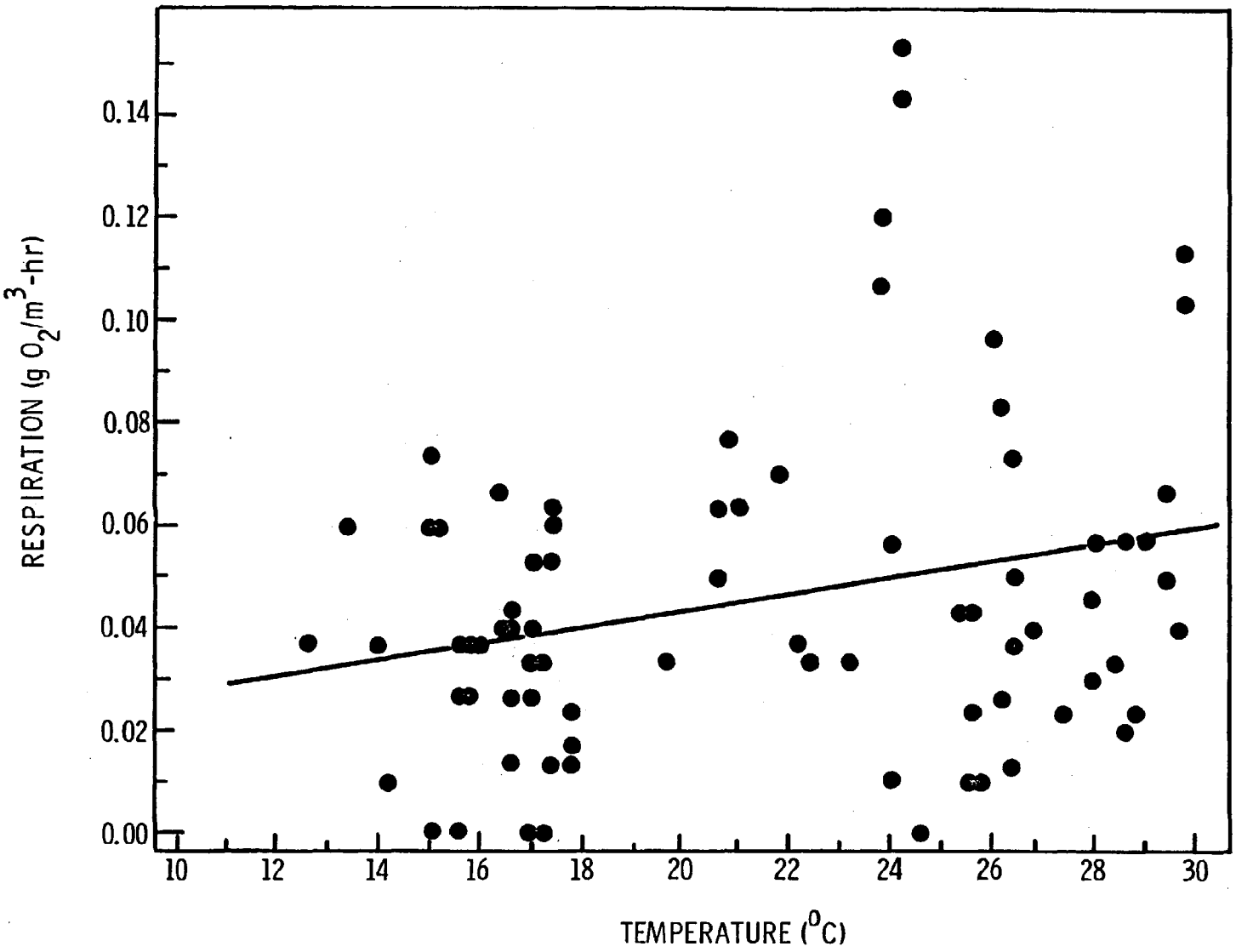

Figure III-6. Respiration of water-column community vs temperature. Line is fitted regression (Eq. 9 and Appendix C)

presented in Appendix C. Since temperatures for the summertime conditions of interest are usually in the range of 25-30°C, this linear approximation should not deviate greatly from the theoretical exponential relationship. The linear relationship (Eq. 9) is substituted into Eq. 4 in all model segments.

Benthic Community Respiration

Estimates of benthic community respiration rates were made in 1980 (Philipp and Klose 1981); these data indicate that benthic respiration may be a major sink for DO. The habitat types represent physical differences among benthic areas observed under low discharge conditions. Means of hourly respiration measurements are grouped by habitat type and date in Fig. III-7, where Habitat 1 represents constantly flowing channel areas; Habitat 2 represents lentic, partially isolated pools at low discharges; and Habitat 3 represents benthic substrate that is exposed to air during shutdown conditions. Standing stocks of periphyton were not estimated, so no data are available about the contribution of differences in biomass to the differences by habitat or date. However, significant differences have been found in the abundance and structure of the macrofaunal community colonizing the three habitat types (Janicki and Ross 1982). The same data, grouped by habitat type vs. distance from the dam (SRBC transects) show similar differences (Fig. III-8). Although there appear to be significant differences in benthic respiration rates among dates, transects, and habitats, it is difficult to apply these data to the DO simulation model. Only 37 respiration measurements were made, and there are few data on the areal extent of each of the three habitats in each of the model segments. Thus, we were forced to use, in Eq. 4, a linear regression equation of respiration rate (g O_2/m^2-hr) as a function of water temperature (°C):

$$R_B = -0.016 + 0.0048T \qquad \text{(Eq. 10)}$$

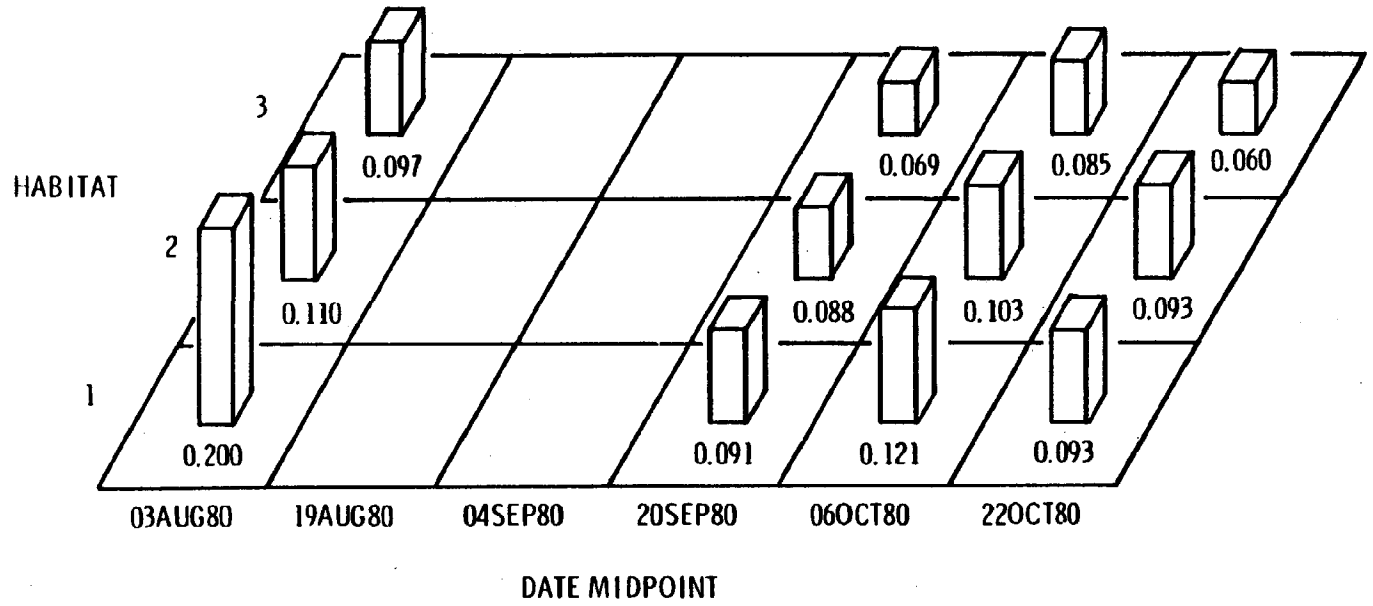

Figure III-7. Means of replicate benthic respiration measurements (g O_2/m^2-hr) by date and hydrologic habitat type: (1) substrate continuously submerged in flowing water; (2) substrate continuously submerged in stagnant pools; (3) substrate intermittently exposed during turbine shutdown periods. Habitat 1 shows highest respiration rate.

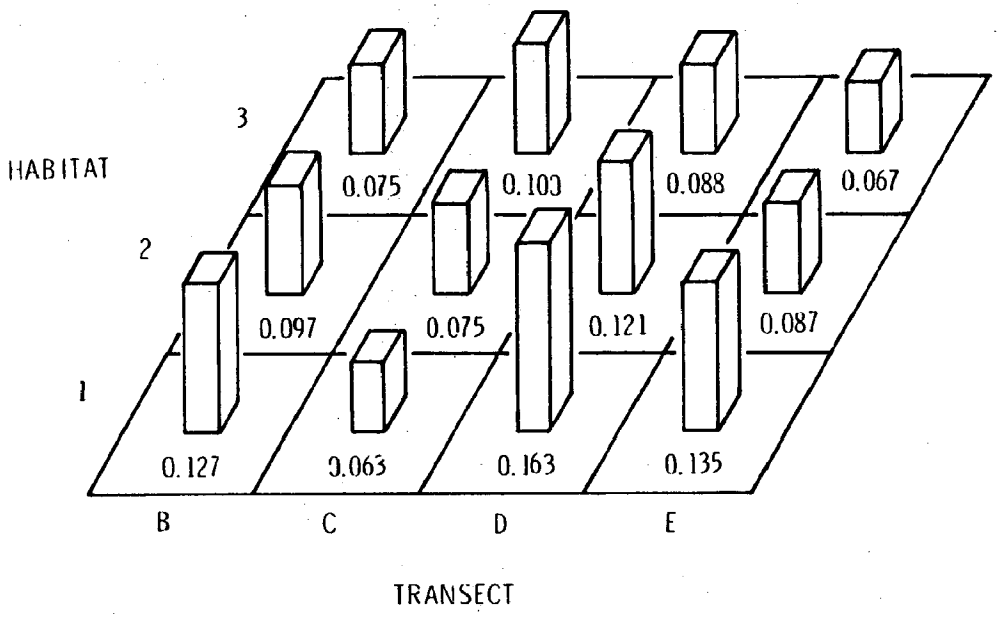

Figure III-8. Means of replicate benthic respiration measurements (g O_2/m^2-hr) by transect and hydrologic habitat type (see Fig. III-7 for habitat descriptions).

Statistics for this regression are presented in Appendix D. This regression is plotted, with raw data, in Fig. III-9. The importance of respiration to overall DO dynamics, and the adequacy of this simple representation, are assessed in Section III.G on sensitivity analyses.

Photosynthetic Oxygen Production

The relationship between the rate of photosynthesis and available light energy is central to the estimation of primary production of oxygen in the river reach. The model uses established general relationships for the dependence of photosynthetic rate on ambient light intensity, and the attenuation of light with water depth, to estimate the oxygen production of both the water-column and benthic communities. This section discusses these relationships in general terms. Subsequent sections present the details of estimating the parameters of the formulation used in the model to relate oxygen production of the water column and benthic communities to ambient light intensity, using measurements made in the river reach during 1980. Those sections also describe the estimation of some input data needed by the model which were not directly measured.

Previous studies (reviewed by Parsons and Takahashi 1973, and Kremer and Nixon 1978) have often shown gross production vs light (hereafter P vs. I) relationships in which the rate of production:

- is light-limited at low I values,
- reaches a (possibly temperature-dependent) maximum (P_{max}) at intermediate I values, or
- sometimes exhibits photoinhibition at high I values.

Steele (1965) introduced a simple equation describing this relationship, which has only two parameters and which remains in common use because of its versatility. The equation describes the reduction of production rate (P) when light intensity (I)

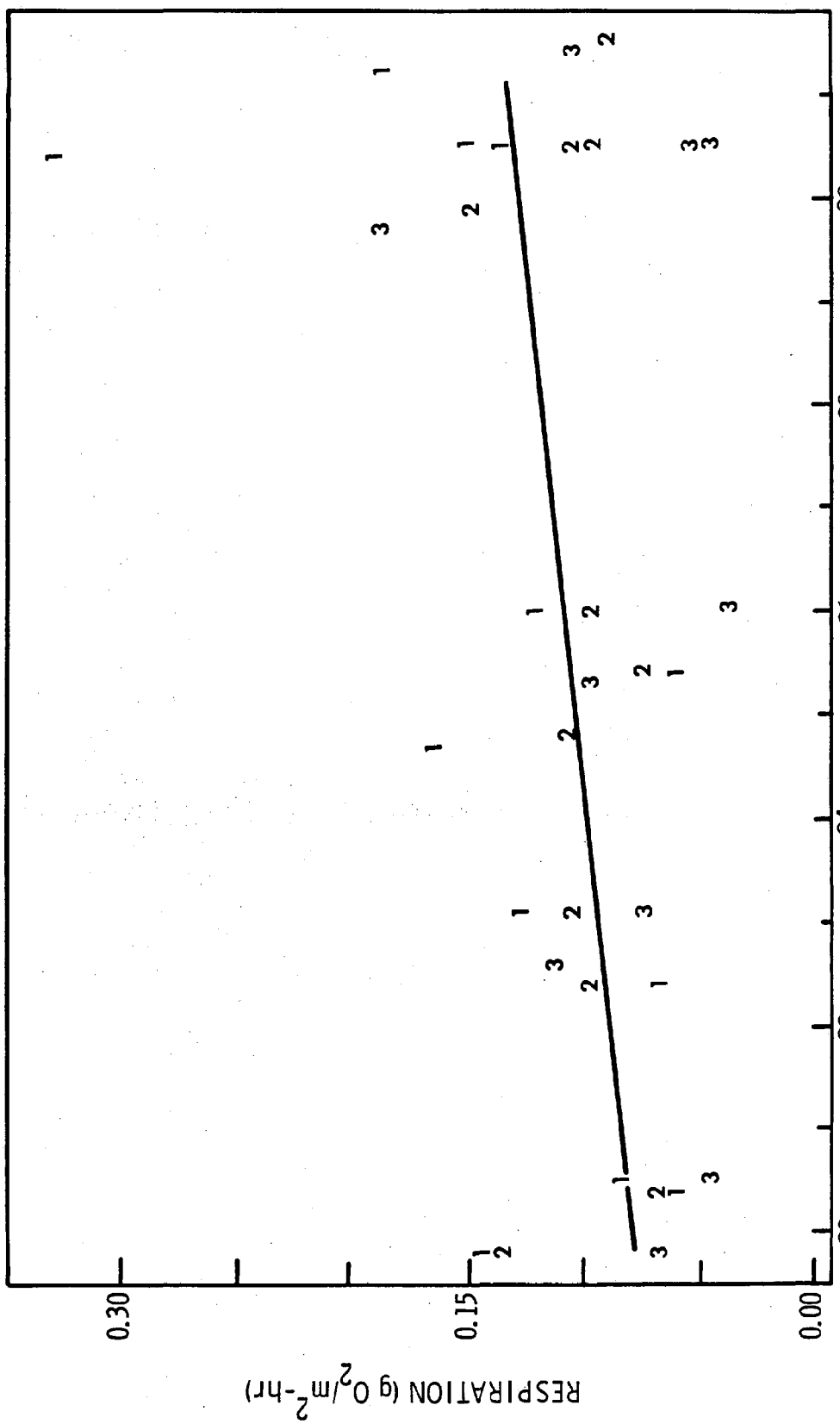

Figure III-9. Benthic community respiration vs. temperature. Symbols are hydrologic habitat type. Line is fitted linear regression (see Appendix D for statistics of regression and Fig. III-7 for habitat descriptions).

is above or below the optimum light intensity (I_{opt}) at which maximum production (P_{max}) is observed:

$$P = P_{max} \frac{I}{I_{opt}} e^{(1-I/I_{opt})}. \qquad \text{(Eq. 11)}$$

The quantity of light energy actually available to algae for phytosynthesis depends on the amount of energy reaching the water surface as a function of time, and on the attenuation of light with water depth due to turbidity. Light energy flux per unit area of water surface (I_o), typically measured in g-cal/cm^2-min (langleys/min), depends on solar angles due to latitude of the measurement point, time of year, and time of day, as well as atmospheric turbidity and cloud cover. Within the water column, light intensity at a depth of z meters (I_z) is related to I_o by:

$$I_z = I_o e^{(-k_{ext} z)}, \qquad \text{(Eq. 12)}$$

which can be substituted directly into Eq. 11 to yield the estimated rate of production at depth z for surface light intensity I_o. The light extinction coefficient (k_{ext}) is related to the depth of disappearance of a 20-cm Secchi disk (z_{Secchi}; Wetzel, 1975) by:

$$k_{ext} = \frac{2.1}{z_{Secchi}}, \qquad \text{(Eq. 13)}$$

which yields $I_z/I_o = 0.122$ at the Secchi-disk depth. Depending on the light absorption characteristics of the water and observer-related variations, values of I_z/I_o at the Secchi-disk depth (the fraction of incident light reaching the Secchi disk) can range from 0.05 to 0.15.

Parameter Estimation for Gross Production of Oxygen by the Water-Column Community

Equations 11-13 provide a versatile mechanism to estimate oxygen production. We used estimates of production made during

1980 in the river reach (Philipp and Klose 1981) to fit the parameters of Eq. 11, after estimating the I_z values during the field incubations. We estimated water-column production of oxygen using the standard light-dark bottle oxygen technique, as described previously for estimating plankton respiration. Net values of water-column oxygen evaluation as large as 0.33 g O_2/m^3-hr, were observed between April and November 1980 (Fig. III-10).

The estimation of I_z, the light intensity to which each light bottle was exposed during incubation, proved to be a complicated process. At the beginning and end of the incubation period during which each light-dark bottle pair was deployed, we made Secchi-disk measurements so we could calculate light intensity at the depth of each pair of light-dark bottles, from the surface light intensity.

Since field measurements of incident light (I_o) were not available for comparison with field productivity measurements, we used known astronomical relationships to estimate the light intensities at the water surface for the time intervals during which the bottle arrays were deployed in the field. This was accomplished by first estimating the angle of the sun above the horizon at the times of interest, using astronomical equations for latitude, time of year, and time of day (Appendix E.1). We used this solar angle in a meteorological equation (Sverdrup et al. 1942; Appendix E.2) to estimate the time-dependent, clear-sky energy flux. We then adjusted the predicted clear-sky value for cloudiness by using the National Weather Service cloud cover data for Baltimore (70 km to the southwest) for the sunrise-to-sunset interval of each day of interest (Appendix E).

However, comparison of Baltimore sunrise-to-sunset values with 3-hour observations of cloud cover indicated that some of the production measurements were done when the cloud cover was very variable during the incubation interval (e.g., changing as much as 90% in 3 hours). Presumably, similar variability affected light intensities near Conowingo Dam on the same days.

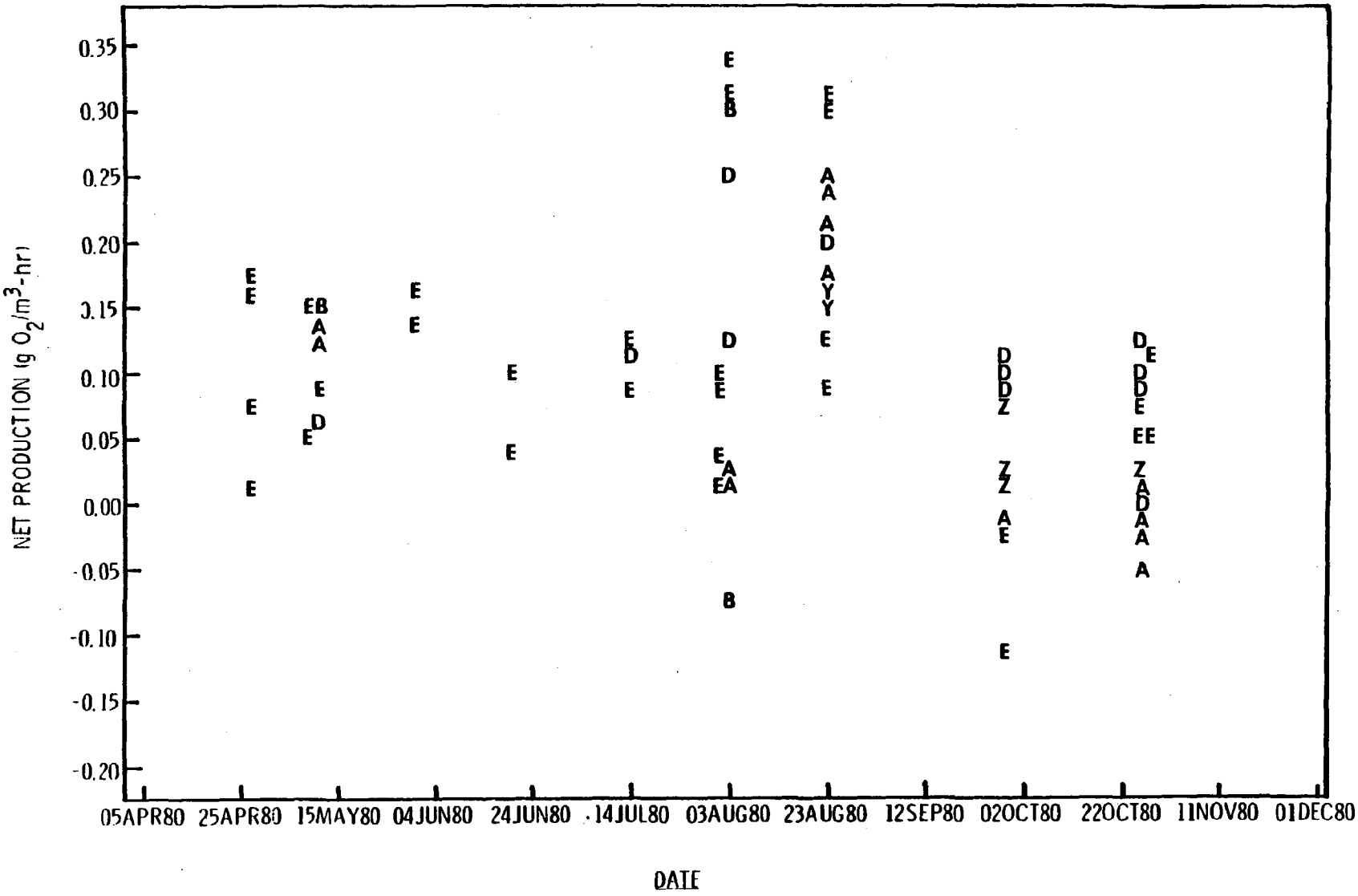

Figure III-10. Estimated net production of water-column community (oxygen evolution), April-October 1980. Data from light-dark bottle incubations at SRBC transects (A-E), and at two stations in the tidal portion of the river (Y, Z).

Thus, our estimates of I_o are subject to some uncertainty. We assess the sensitivity of modelled DO values to variations in I_o in a later section.

We estimated I_z values from I_o using the Secchi-disk measurements made in the field. Secchi-disk measurements made during the incubations proved to be variable, changing as much as 1 m between the beginning and end of a single 8-hr incubation. The mean value was 0.65 m for all measurements at all discharges, which ranged from 0.2 to 2.2 m. Values of Secchi-disk depth showed no relation to either natural river flow or turbine discharge. Due to the exponential nature of the light attenuation relationship (Eq. 12), small errors or changes in Secchi-disk depth measurements can result in very large errors in the estimates of light reaching the bottle arrays. For example, a change in Secchi-disk depth from the average value of 0.65 m to 0.83 m results in a 100% increase in the light intensity reaching a depth of 1 m. The effects of variations in Secchi-disk depth on output DO values are assessed in the sensitivity analysis section.

In spite of these difficulties, the values of average I_z calculated for each of the light bottle incubations represent the best possible estimates of water column production with available information, and can certainly be used to examine relative production rates vs. light. Figure III-11 plots gross production rates of oxygen (g O_2/m^3-min) from 90 light-dark bottle pairs against our best estimates of average I_z (ly/min) during each of the incubations (calculated as previously described). The data show the expected maximum at intermediate light intensities (near 0.15 ly/min). Because we expected that P_{max} would depend on temperature, we separated the gross production data into two temperature groups and fitted the Steele equation (Eq. 11) to each group, yielding the following sets of parameter estimates:

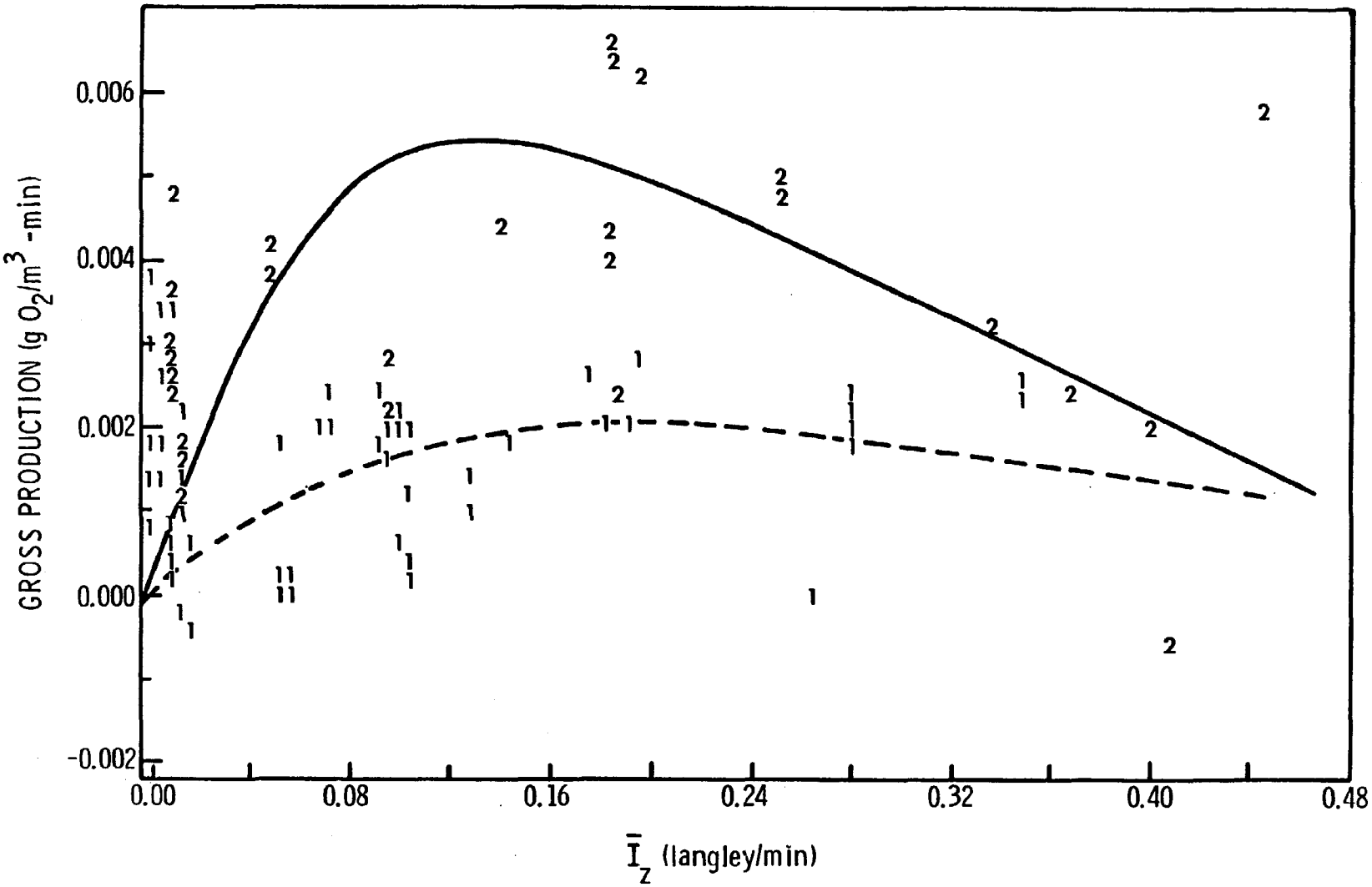

Figure III-11. Gross oxygen production vs. estimated average light intensities at the depth and time of light-dark bottle incubations: 1's and dashed line are data, and fitted regression of Steele equation (Eq. 11), respectively, to gross production estimates at water temperatures less than or equal to 25°C; 2's and solid line are data, and fitted regression of Eq. 11 to estimates at temperatures greater than 25°C (statistics for regressions are in Appendix F).

T (°C)	P_{max} (g O_2/m^3-min)	I_{opt} (ly/min)
$\leq$ 25	0.0020	0.15
> 25	0.0054	0.15

Simulations of summer conditions, which are the focus of interest here, will generally use the second pair of coefficients (> 25°C).

The model algorithm for water-column algal production integrates Eq. 11 (after substitution of Eqs. 12 and 13) between the surface and bottom depths (estimated by USTFLO), using a Runge-Kutta numerical integration scheme. This calculation uses an instantaneous I_o calculated from sun angle for that time and the National Weather Service (Baltimore) estimate for average cloud cover for that day. A value for I_z is calculated from I_o and average Secchi-disk depth. This rate of water-column production is substituted for DP_{WC} in Eq. 4.

Estimation of Gross Production of the Benthic Community

Production vs. light relationships for benthic algae could not be estimated from field data. Measurements of benthic production were done by transporting periphyton-covered cobble-sized rocks to sealed chambers in water baths on shore. The turbidity of the overlying cooling water was very variable, and the light attenuation characteristics of the chamber and water within it were not measured. However, we were able to fit (by eye) a relationship between temperature and the highest values for benthic gross production measured in 1980 (i.e., the six measurements made under midday light conditions; circled in Fig. III-12):

$$P_{max} = 0.1 + 0.02\ T \qquad \text{(Eq. 14)}$$

where T is temperature (°C).

Since we could not use the 1980 benthic productivity data to estimate I_{opt}, our only alternative was to find literature values for I_{opt} from other systems. Phinney and McIntire (1965)

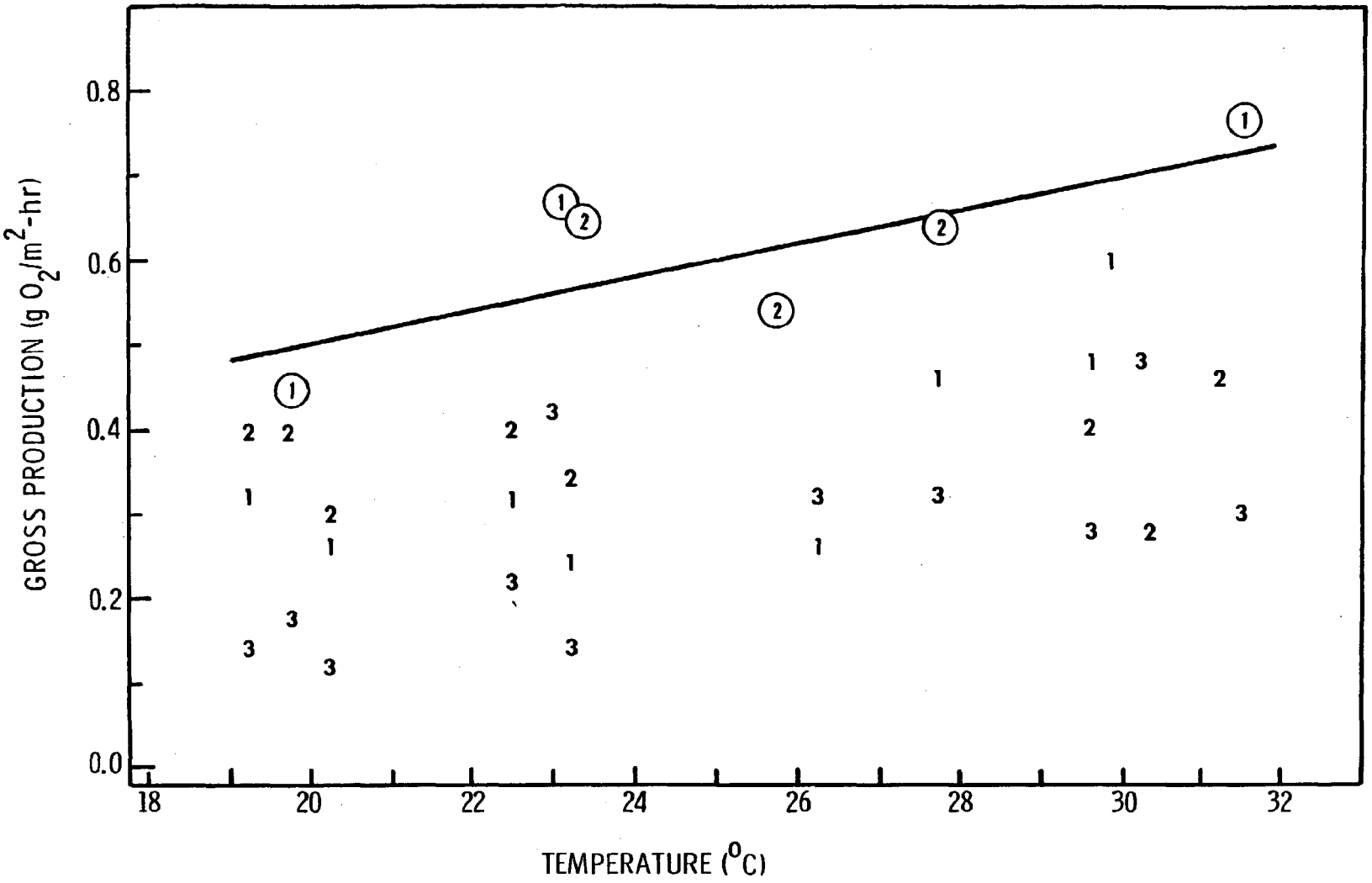

Figure III-12. Gross oxygen production of the benthic community vs. temperature. Line estimates P max vs. temperature for the benthic community (Eq. 14), and was fitted by eye through the six measurements made under midday full sunlight conditions (points in circles). Numbers denote habitat type (see Fig. III-7).

measured periphyton production in artificial streams maintained in flumes under artificial illumination at two different temperatures. The light intensities produced by the incandescent lamps ranged from 0.01 to 0.15 ly/min, which is much lower than intensities observed in natural daylight. Consequently, their production vs. light curves do not show photoinhibition, which prevents estimating I_{opt} from their data. (In contrast, P_{max} values at two temperatures from their data closely fit the P_{max} estimated by Eq. 14 above.) We found no other production vs light data for periphyton in the literature. Consequently, we set the I_{opt} value for the benthos at 0.15 (the same as estimated for water-column algae) as a first approximation, and adjusted it later during the calibration of the model.

The algorithm finally used to simulate benthic algal production calculates oxygen production from Eq. 11, after substituting Eq. 14, average segment depth (from USTFLO), I_o, and I_z as we did with water-column algal production. We substituted this rate for P_b in Eq. 4, making the assumption that the benthic surface area was equal to water surface area (S) in this wide, shallow river reach.

D. CALIBRATION OF PARAMETERS IN THE DO MODEL

The primary purpose of the DO model is to estimate DO distributions in the river during the periods of the year when turbine shutdowns accompanied by depletion of DO downstream (i.e., DO levels less than 4 ppm) are likely to occur. Field measurements during 1980 and 1981 indicated that such conditions occurred primarily during summer and early fall (June to early October). As discussed in Section III.C above, we drew a number of initial parameter estimates from field measurements of processes, which were made primarily during the summer of 1980, a period of low natural river flow when periods of turbine shutdown were common. To calibrate the model, we compared simulated DO (using these initial estimates) to observed DO values and subsequently

adjusted the parameters to correct for any lack of fit. This calibration was accomplished using continuous DO data for a three-day interval (5-7 July 1980) from the same period that shows a typical discharge pattern for summer. The monitor data were taken at the dam discharge (actually a cooling line which draws water from the reservoir near a turbine intake) and in a flowing channel area at the fall line (Philipp and Klose 1981). We used time-series DO from the cooling line and flow data at the dam discharge as inputs and adjusted model parameters as necessary so that simulated DO concentrations at transect A (the fall line; Fig. II-1) matched observed DO values at the fall-line monitor. Measured dam discharge for this period is shown in Fig. III-13a, and the DO of the cooling line vs DO from the fall-line monitor are shown in Fig. III-13b.

On each of the three days during morning shutdown periods, measured DO values at the fall line (transect A) increased rapidly in early morning. On the second day (a Sunday), continuation of the shutdown throughout the day caused DO to maintain a plateau near 9 ppm. In the initial calibration runs, the simulated fall-line DO fit the observed DO quite well. However, the individual production rates (P_B and DP_{WC}) in the initial runs exhibited severe photoinhibition during much of the day.

This photoinhibition is controlled by the relation between the ambient light intensity (I_z) and the photosynthetic optimum intensity (I_{opt}). Measurements of Secchi-disk depth (which partially determines I_z) in 1980 showed considerable variation over periods as short as a few hours (Philipp and Klose 1981). Also, the initial estimate of I_{opt} = 0.15 ly/min was much lower than other values reported in the literature. To investigate the sensitivity of the model's production mechanism to variations in these light parameters, or errors in their estimation, we solved the benthic production equation (Eq. 11 calculated at water depth z = 1.0 m) hourly from dawn to dusk for all combinations of Secchi-depth values of 0.2, 0.7, 1.2, 1.7, and 2.2 plus I_{opt} values of 0.15, 0.3, and 0.5. This yielded 15 parameterized

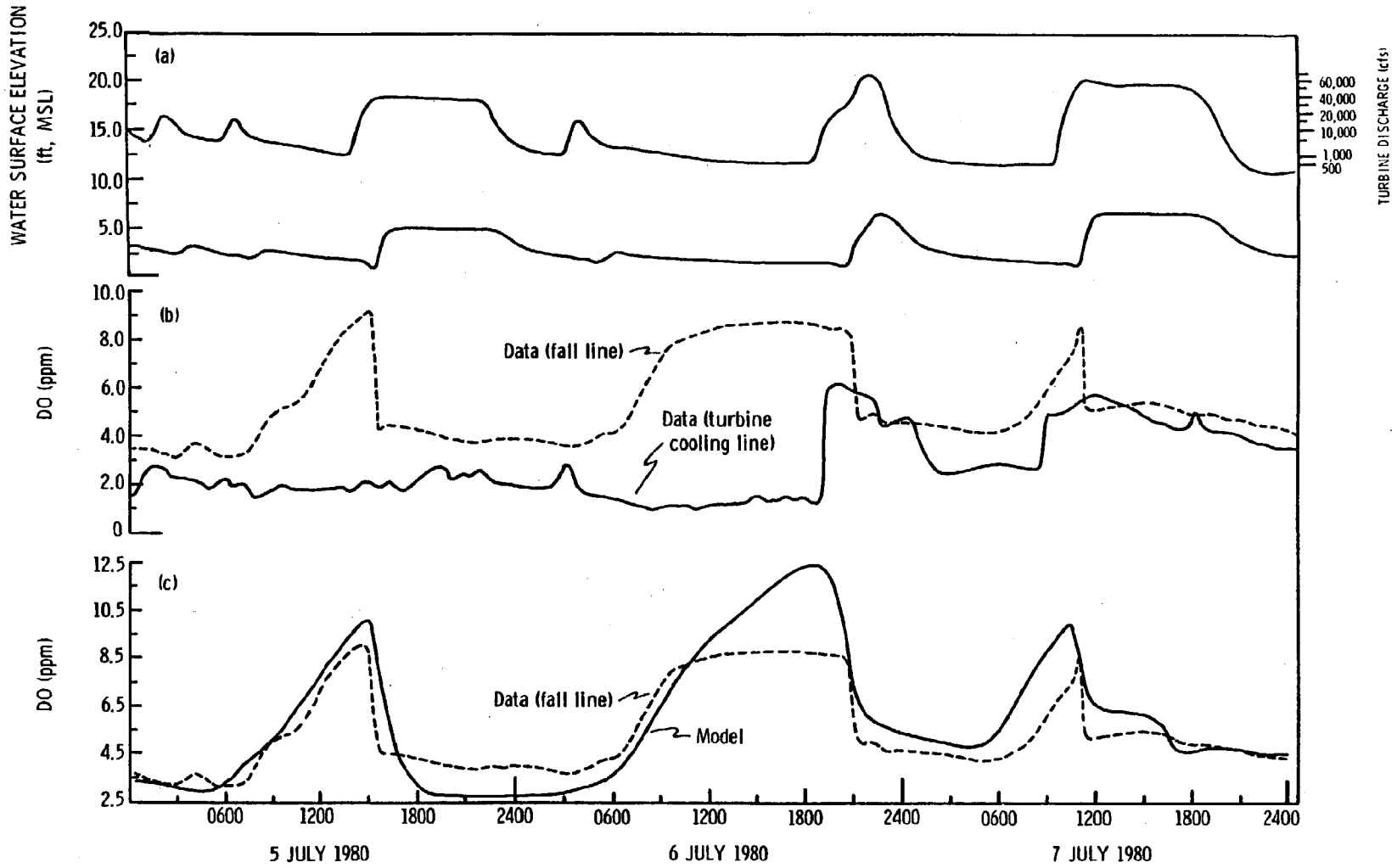

Figure III-13. Calibration of the DO model, 5-7 July 1980

(a) Simulated water surface elevation and corresponding discharge at the dam (upper solid line) and simulated elevations at the fall line (lower solid line).

(b) DO of the discharge (cooling line of the #2 turbine-solid line), and DO measured at the fall line (dashed line).

(c) DO measured at the fall line [dashed line, same as in (b) above], and DO at the fall line simulated by the model (solid line).

curves of benthic production rate under a wide range of I_z values and differing sensitivities of photosynthesis to light. The curves for I_{opt} = 0.15 and 0.5 are shown in Figs. III-14a and III-14b, respectively. The curves of Fig. III-14a show that oxygen production is very sensitive to the light intensity reaching the benthos when I_{opt} = 0.15. For instance, an increase in Secchi-disk depth from 0.7 m to 1.2 m causes the light level at a depth of 1 m to increase by a factor of 3.5. At the 1.2 m Secchi-disk depth, the rate of photosynthesis becomes inhibited by light at unrealistically low light levels (e.g., those occurring after 7:00 a.m.; see Fig. III-14a). This is a marked change from the diel pattern of photosynthesis shown for the 0.7 m Secchi-disk depth.

Actual Secchi-disk depths commonly varied by ± 0.5 m during day, and could easily have varied by more than that during the 5-7 July calibration interval. Thus, it was desirable to decrease the sensitivity of photosynthesis to such unknown variations in available light while maintaining the general daily pattern exhibited by the combination of I_{opt} = 0.15 and Secchi-disk depth = 0.65. In Fig. III-14b (I_{opt} = 0.5), the effects of photoinhibition are less pronounced. Secchi-disk depths of 1.2 to 2.2 all maintain a general daily production pattern similar to that observed with I_{opt} = 0.15, Secchi-disk depth = 0.65. Accordingly, we selected new combinations of light parameters (I_{opt} = 0.5, Secchi-disk depth = 1.7 m) to determine if they improved the fit of simulations.

Although the new parameter values differ from those derived from field measurements, there is justification for their use in the model. A review of a large body of literature (Nixon et al. 1979) indicates that an I_{opt} value of 0.5 ly/min is in the range of values from a number of different ecosystems. The new value for Secchi-disk depth (1.7 m) used in the model is well within the range of values measured in the river reach during the summer of 1980. During shutdown or low discharge periods, when in situ oxygen production likely has the greatest relative

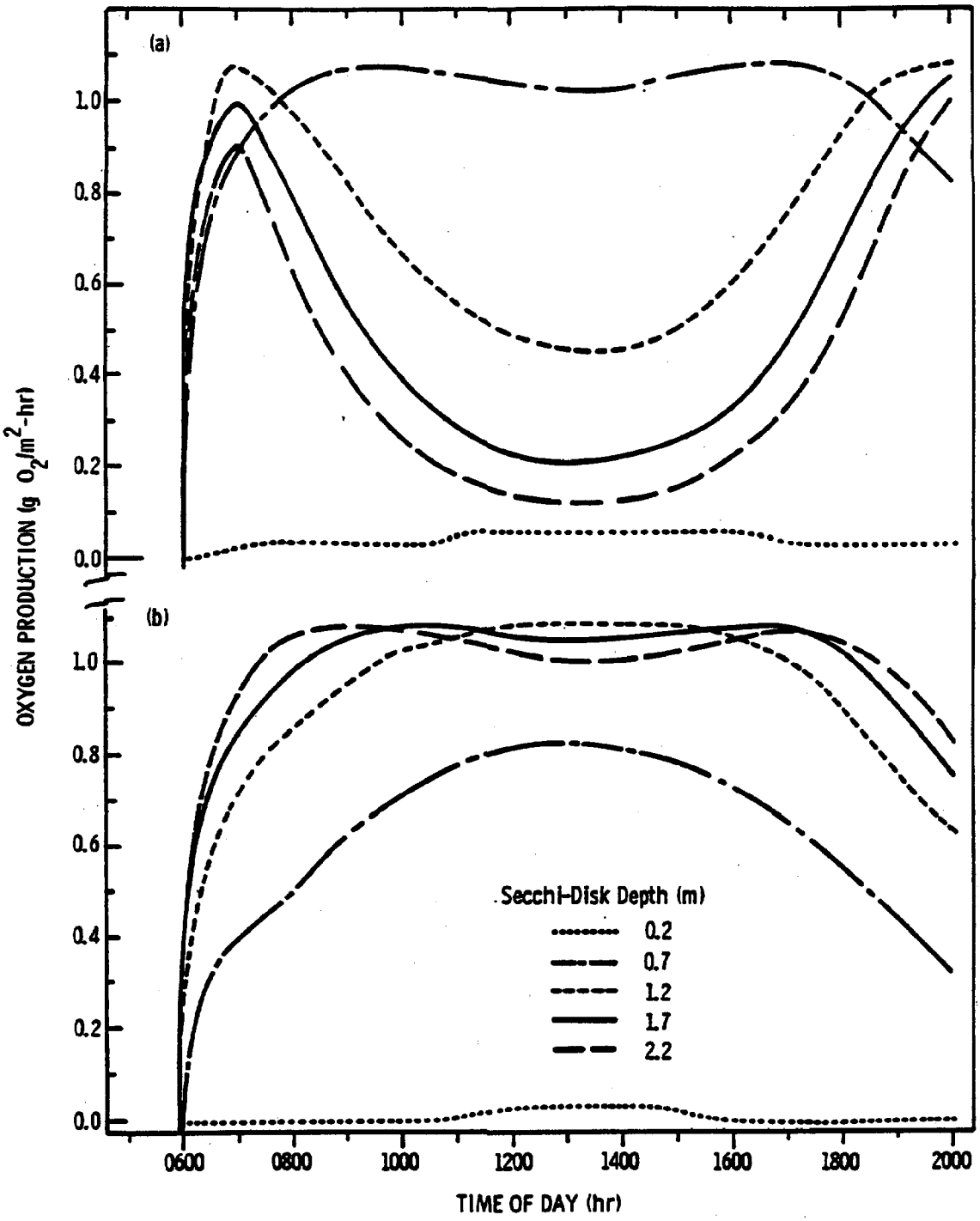

Figure III-14. Sensitivity over a day (time is hour of the day) of simulated benthic oxygen production to different values of I_{opt} and Secchi-disk depth.
(a) Benthic production at depth of 1 m, I_{opt} = 0.15 ly/min. Production shows pronounced photoinhibition for all Secchi-disk depths greater than 0.7 m (i.e., for relatively non-turbid water).
(b) benthic production (1-m depth) for I_{opt} = 0.5 ly/min. Production at Secchi-disk depths of 0.7, 1.2, and 1.7 m all show similar production curves, without extreme photoinhibition.

effect on DO values in the river, the lack of water turbulence probably permits an appreciable amount of suspended sediment to settle out. This would likely decrease the turbidity of the water, and increase Secchi-disk depths above the average value of 0.65 m.

We reran the oxygen model with the new values of I_{opt} = 0.5 (both for water-column and benthic production) and Secchi-disk depth = 1.7 m. A comparison of simulated vs. observed DO values at transect A (Fig. III-13c) shows that simulated increases in morning DO during shutdown periods generally follow observed rates of DO increase. However, some significant discrepancies are evident. Simulated DO values on the afternoon of the second day (6 July) are significantly higher (~ 3.5 ppm) than values observed at the transect A monitor. This phenomenon can be explained by considering the differences found between model DO values, which are estimates of average DO concentrations within segments, and point DO measurements. At low discharges, such point measurements generally characterize the DO distributions of individual nonflowing pools, and the data show large pool-to-pool variations (Philipp and Klose 1981). In contrast, the DO monitor at transect A is in a continuously flowing channel, where it records the DO of water that has traveled through the river reach in minimum time. Thus, increases in DO values measured in channel areas are likely to be low relative to those in slower waters or nonflowing pool areas, since production has had a relatively short time to increase DO.

Measured discharges (Fig. III-13a) during these daytime DO peaks (Fig. III-13c) appear to represent the lowest flows observed in the record (i.e., when discharge is much lower than 1,000 cfs). Thus, it appears that the discrepancy between simulated and observed DO values may be largest when the model attempts to simulate very shallow waters or very low flow conditions. It will be necessary to monitor DO values in some of the slow-flowing pools in order to recalibrate the model so that it fits shut-down conditions.

Another significant discrepancy between observed and simulated DO values occurs during some periods of full discharge (Fig. III-13c). During the first full-discharge period (1600-2300, 5 July), observed DO values are about 1 ppm higher than simulated values. Conversely, observed values are lower than simulated during the next peaking discharge (1900-2400, 6 July). Since cross-stream DO variation during periods of full discharge is negligible (Philipp and Klose 1981), the differences cannot be explained by the monitor data not being representative of average DO values in the river, as may be the case during shutdown periods.

An alternate explanation is that the DO measured at the cooling line is not an accurate estimate of water discharged by the turbines. There is evidence that DO data from the cooling lines are not representative of the DO of the discharge water, particularly at low discharges (Philipp and Klose 1981; RMC, in prep.). Any errors in estimating input DO values will result in discrepancies downstream. We are presently attempting to obtain a better estimate of the discharge DO from analyses of reservoir and other DO data.

The incorrect estimation of input DO also can explain the 2.5-ppm difference in DO between observed and simulated values for the morning shutdown on the third day (Fig. III-13c). The shapes of the peaks (i.e., rate of DO production) of the two curves are similar, but there is a relatively constant offset in the peak for the third day. It could well be that this difference in DO is a continuation of the difference evident during the previous night, which was probably caused by the inaccurate estimation of input DO during the nighttime peak discharge.

To summarize model calibration, we only needed to adjust two parameters relating production to light to improve the fit of the model to observed data. Some discrepancies between simulated and observed DO values appear to be related to problems with the representativeness of point measurements of DO data.

At low discharges, the downstream DO monitor may underestimate average DO values in the river. However, the model appears to simulate typical patterns of daytime oxygen production observed in pools during shutdowns. The accuracy of model estimates of average river DO under such conditions cannot be assessed with the data presently available. At full discharges, errors in estimates of input DO have the greatest effect on simulated DO values downstream, simply because of the volume of the discharge relative to that in the river reach, and because very short residence times prevent in situ processes from appreciably affecting DO. This should not affect the usefulness of the model for assessing suitability of biotic habitat, because deleterious effects on biota are not usually associated with full-discharge conditions. With the field data presently available, it is unlikely that any further refinements of the DO model could improve the fit between simulated and observed values. Model resolution and accuracy can be improved only with the collection of additional data.

E. VALIDATION OF THE DO MODEL

Validation of a simulation model consists of comparisons of simulated output with observed data that are independent of those used in model calibration. Because the continuous monitor records for the summer of 1981 are independent of the 1980 data used in model calibration, we selected two time intervals from 1981: 27-28 June 1981, when turbine discharge was at a minimum continuous level of 5,000 cfs; and 25 July-2 August 1981, when daily intervals of turbine shutdown occurred.

However, on 6 July 1981, PECO instituted a new type of discharge regime consisting of setting the maximum duration of shutdown periods at 8 hours, and using discharge periods of a minimum of 5,000 cfs for at least four hours. A variation of this regime, used during the second validation interval (25 July-2 August 1981), did not have prolonged shutdown periods such as those used during summers prior to 1981.

Validation runs against 1981 data thus evaluate the model fit relative to high flow (continuous discharge) conditions, as well as conditions under the PECO regime. To validate the model for periods of river flow lower than observed in 1981 and normal turbine operation (peaking followed by long shutdowns), we had to apply data from the summer of 1980. Accordingly, we made a third validation run using monitor data from 8-10 July 1980. In a strict sense, this period cannot be considered appropriate for true model validation because it is part of the summer of intensive field sampling done to calibrate the model. However, no data taken during 8-10 July were subsequently used in calibrating the model. We thus feel that data from this period are independent of calibrating data, although they have been influenced by the general river flows and meteorological conditions that characterized the calibration period.

To assess the fit of the model to DO data at transect A, we defined several quantitative indices. First, we calculated a mean value of simulated DO minus observed DO (ΔDO) using all simulated points of each run. Since ΔDO values can be both positive and negative, the mean of ΔDO tends to under-estimate lack of fit. Accordingly, we also calculated the mean of $|\Delta DO|$. Then we calculated variances of ΔDO and $|\Delta DO|$, as well as the range of ΔDO. Equivalent statistics were calculated for both temperature and water height. Calculated indices for all three variables for the three validation runs are presented in Table III-2. We made no attempt to calculate these statistics as a function of discharge, or to analyze the data for time periods shorter than the length of the simulation run.

The 27-28 June 1981 run encompassed a Saturday-Sunday period with a minimum discharge of 6,400 cfs (Fig. III-15a). During this period, DO values of the input (the cooling line) and transect A were similar, and remained in the range of 6-8 ppm (Fig. III-15b). Simulated DO values at transect A were always higher than observed values (Fig. III-15c). Estimates of mean ΔDO and $|\Delta DO|$ (Table III-2) were similar ($\sim$ 0.89 ppm)

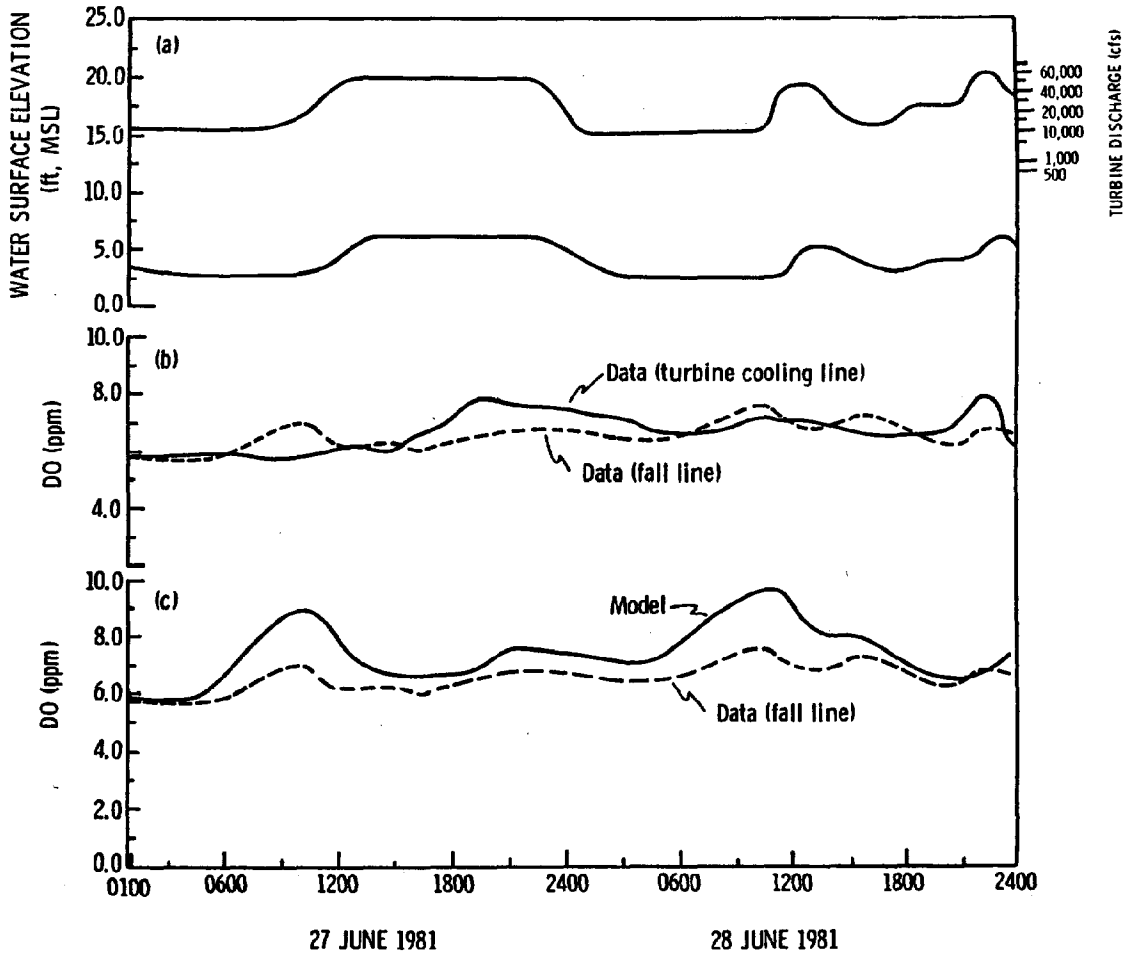

Figure III-15. Validation of the DO model, for the continuous discharge period, 27-28 June 1981.

(a) Simulated water surface elevation at the dam (upper solid line), and simulated elevation at the fall line (lower solid line).

(b) DO of the cooling line of the #2 turbine (solid line), and DO measured at the fall line (dashed line).

(c) DO measured at the fall line [dashed line; same as in (b) above], and DO at the fall line simulated by the model (solid line).

Table III-2. Estimates of average differences between simulated and actual values for system outputs for three validation runs

	ΔDO (ppm) (simulated minus actual)	|ΔDO|	ΔT (°C) (simulated minus actual)	|ΔT|	ΔH (ft) (simulated minus actual)	|ΔH|
27-28 June 1981						
Mean	0.89	0.90	1.30	1.32	-0.0808	0.121
Variance	0.41	0.40	0.71	0.65	0.0283	0.020
Maximum	2.64	--	2.88	--	0.24	--
Minimum	-0.27	--	-0.40	--	-0.90	--
25 July-2 August 1981						
Mean	-0.16	0.59	1.13	1.36	-0.0125	0.146
Variance	0.60	0.28	1.29	0.72	0.0403	0.019
Maximum	4.83	--	3.76	--	0.55	--
Minimum	-2.19	--	-1.60	--	-1.31	--
8-10 July 1980						
Mean	0.53	0.68	2.26	2.06	no measurement	
Variance	0.61	0.43	2.64	3.49	of H in 1980	
Maximum	4.00	--	6.30	--		
Minimum	-0.84	--	-1.10	--		

because the error was usually in the same direction. This bias is reflected in the range of ΔDO. As can be seen in Fig. III-15c, ΔDO is greatest during daylight, suggesting that the high DO values are due to too large a rate of oxygen production. High river flow or continuous discharge by the turbines could cause continuous mixing of the water in the reservoir and in the river reach, thus preventing any settling of suspended solids. High turbidity due to mixing would depress actual oxygen production in the river reach, so the use of an average Secchi-disk depth characteristic of slower flowing conditions, would tend to cause the model to overestimate DO during daylight hours relative to actual values.

Thus, under conditions of high river flow and continuous discharge, the model reproduces daily fluctuations in DO, but on the average it appears to consistently overestimate DO by slightly less than 1 ppm. Therefore, if it is necessary to use the model to simulate conditions of high river flow, it probably will be helpful to acquire more or better data (i.e., on the variation of turbidity with flow) so model mechanisms can be appropriately reformulated and recalibrated.

Although the model is not intended to simulate water temperature, a number of oxygen rate processes are controlled by temperature. Thus, it is useful to examine the fit of the algorithm for diel temperature change to data from transect A. Values for ΔT (Table III-2) during this continuous discharge period appear to be within 1.3°C of actual data, and such a small difference is not likely to significantly affect metabolic rates.

We also compared simulated elevations in water surface at transect A with actual data to assure that USTFLO was generating correct hydrodynamic inputs to the oxygen model. During the period 27-28 June 1981, ΔH and $|\Delta H|$ were on the average 1-1.5 inches from observed data (Table III-2).

The second validation period (25 July to 2 August 1981) was a period of normal summer river discharges. The turbines

operated on a peaking schedule, with nighttime and weekend shutdown intervals. Long shutdown periods were interrupted with 1-hour pulse discharges of 5,000 cfs every 5 hours (Fig. III-16a). Even under this discharge regime, simulated water heights closely fit observed data (Table III-2).

As discussed above, the cooling-line DO data are at times unsatisfactory as the input DO values for the model. However, for the 25 July-2 August period, another DO record is available as an alternative input -- the DO concentration at 10 m depth in the reservoir (near the top of the intake penstocks for the turbines). These data are likely to be representative of the DO of some portion of the water withdrawn by the turbines, and they follow the general trend shown by cooling-line DO data. In addition, the data are not subject to short-term DO depressions due to localized oxygen consumption in the penstock and cooling line during shutdowns. Accordingly, we used this reservoir DO record as the DO of input water for this simulation (Fig. III-16b). The record of the DO monitor in the cooling line of the #5 turbine is also shown in Fig III-16b for comparative purposes.

Simulated DO concentrations at transect A appear to closely fit observed data (Fig. III-16c), averaging a 0.6 ppm difference (ΔDO) between the two data sets (Table III-1). As indicated during the calibration run, the DO record in the channel at transect A may not be a good representation of the average DO of the river (as simulated by the model) during daytime shutdown periods. The range of ΔDO for this run (up to 4.8 ppm; Table III-3 and Fig. III-16c) indicates that the model ocassionally overestimates the data from transect A. However, as previously discussed, such high simulated DO values may be indicative of real DO values in the predominant pool areas of the river, but no data exist to test this hypothesis. No bias is evident in ΔDO over the entire run. Thus, the model appears to adequately fit the DO values observed over the 9-day period.

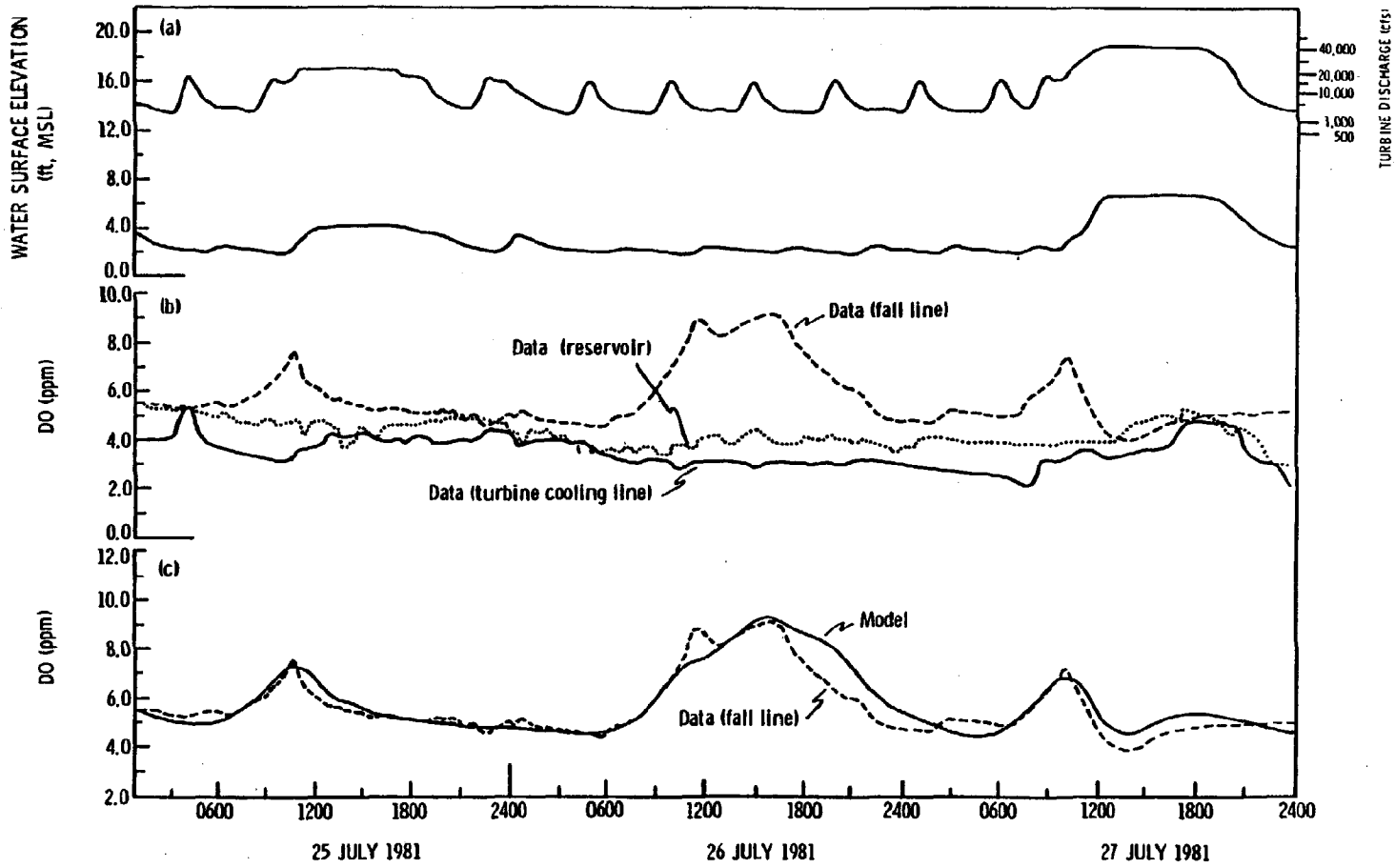

Figure III-16. Validation of the DO model, 25 July-2 August 1981

(a) Simulated water surface elevation, and corresponding discharge at the dam (upper solid line), and simulated elevations at the fall line (lower (solid line).

(b) Two estimates of the DO of the discharge (cooling line of the #5 turbine - solid line; reservoir at 10 m depth - dotted line), and DO measured at the fall line (dashed line).

(c) DO measured at the fall line [dashed line, same as in (b) above], and DO at the fall line simulated by the model (solid line).

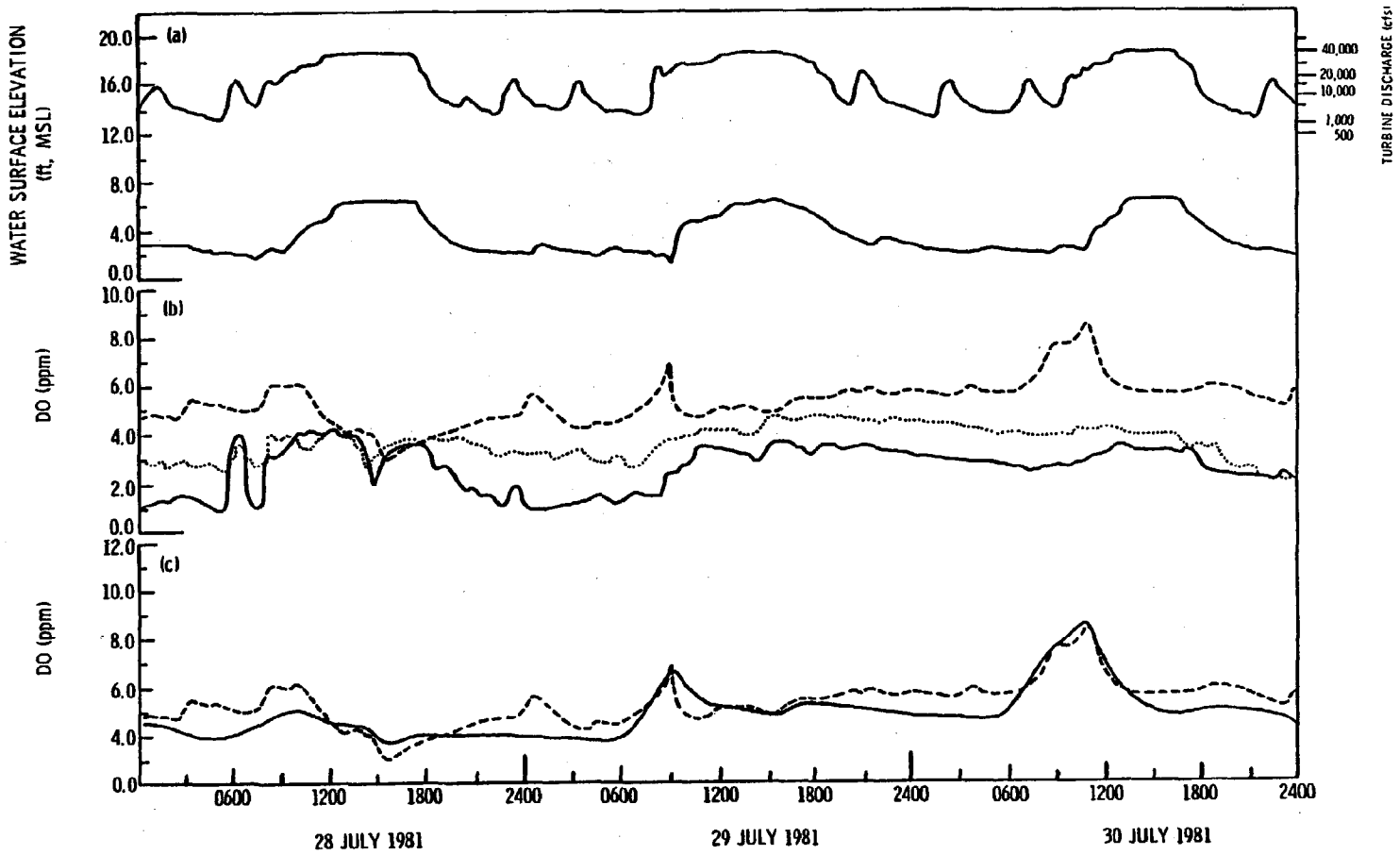

Figure III-16. Continued.

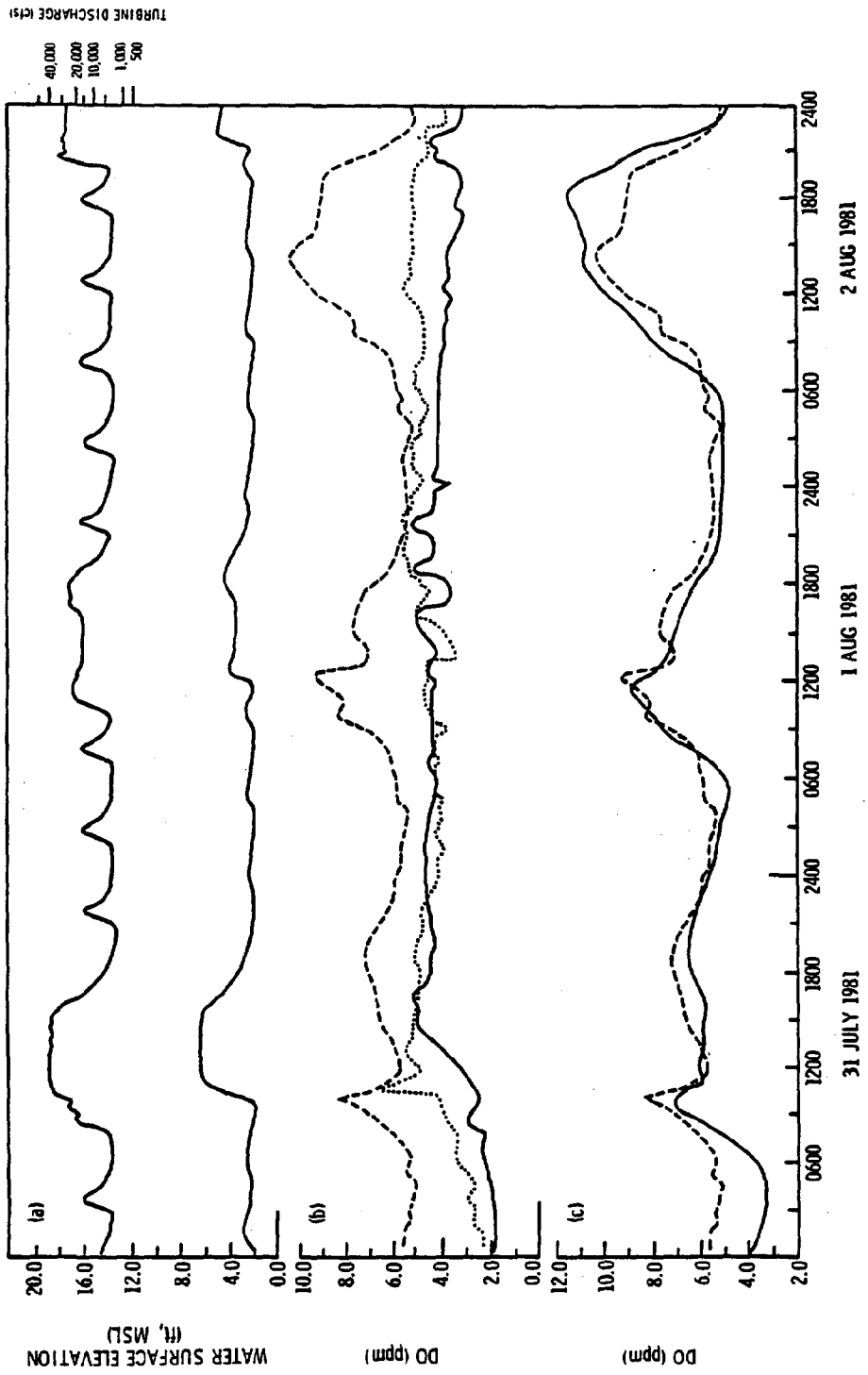

Figure III-16. Continued.

Table III-3. Relative contributions of individual rate processes (%) to the average DO concentration at the downstream (fall line) boundary over two periods.

	27-28 June 1981	25 July-2 August 1981
Average natural river flow (cfs)	23,057	13,065
Relative contribution (%) of:		
Discharge DO	90.6	75.5
Benthic Community		
--Production	7.7	15.4
--Respiration	-3.6	-9.9
Reaeration	2.3	13.3
Water-Column Community		
--Production	4.3	7.9
--Respiration	-1.9	-3.8

Simulated values for water temperature and height at transect A agree with observed data, as shown by average values of $|\Delta T| = 1.36°C$ and $|\Delta H| = 0.15$ ft (Table III-2). Such differences are again not significant.

These two simulations of periods during 1981 assessed the fit of the model to DO under continuous high flow conditions, and to DO affected by PECO's pulsing discharge regime. In contrast, the third validation period (8-10 July 1980) is characterized by low natural river flows and shutdown periods not affected by PECO's pulsing discharge schedule (Fig. III-17a). The input data (in this case, from cooling line monitors) again show abrupt changes in DO in response to discharge changes (Fig. III-17b), which affect simulated DO values at transect A (Fig. III-17c). In spite of this the model generally fits observed DO data at transect A (Table III-2), with relatively large deviations occurring only during daytime under shutdown conditions much lower than 1,000 cfs.

To summarize our discussion of validation of the DO model, it is useful to consider the conditions under which the model agrees with, or deviates from, observed DO values at transect A. First, the model appears to fit (defined arbitrarily as $|\Delta DO| < 1$ ppm) data taken during any summer intervals characterized by shutdown conditions, as shown by the validation runs of 25 July-2 August 1981, and 8-10 July 1980. These conditions are of primary importance if the model is to be used as a management tool, for instance, to estimate the relative effects of some hypothetical minimum discharge scenarios.

Although reaeration at the turbine discharge boils may have an effect on the accuracy of the DO at the upstream boundary, we saw no evidence that any such reaeration consistently affected the fit of the model to measured DO values at transect D (not shown). We expect that this reaeration term is small, on the order of the error inherent in the measurements of DO at the turbines.

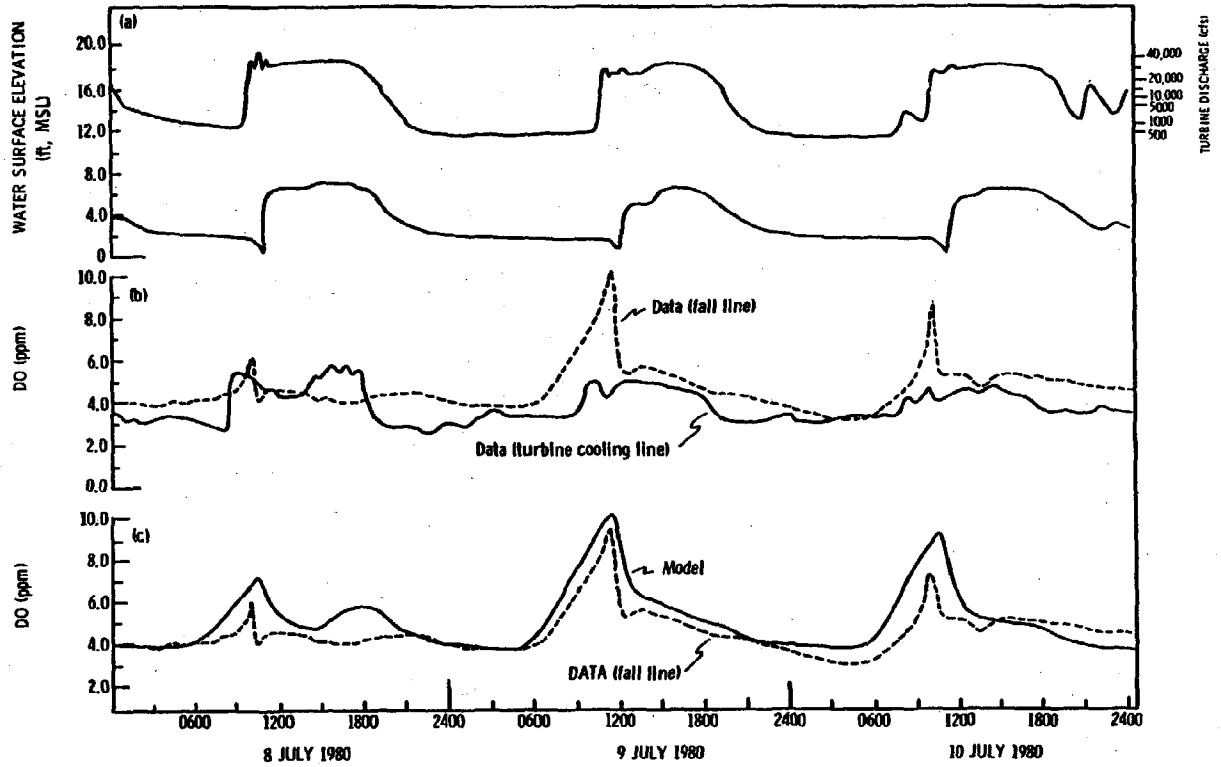

Figure III-17. Validation of the DO model, 8-10 July 1980

(a) Simulated water surface elevation and corresponding discharge at the dam (upper solid line), and simulated elevations at the fall line (lower (solid line).

(b) DO of the discharge (cooling line of the #2 turbine - solid line) line), and DO measured at the fall line (dashed line).

(c) DO measured at the fall line [dashed line, same as in (b) above] and DO at the fall line simulated by the model (solid line).

There are, however, certain instances when the simulated average DO values do not agree with observed data. The following are the only significant deviations we could find, and they make up only a small percentage of the total period of the simulation runs. The first difference occurs during some daytime shutdown conditions when DO conditions over a large portion of the river show much spatial variation. Also, the model overestimates DO values during periods of high river flow (e.g., 27-28 June 1981) when increased turbidity (not accounted for by the model) may decrease actual oxygen production. Another problem causing lack of fit at times is the possible unrepresentativeness of the cooling-line DO data used to estimate the DO concentration of input water from the dam discharge. We are presently investigating alternative means of calculating input DO.

In spite of minor deviations from observed data under certain conditions, the model appears to validly simulate average DO distributions in the river reach during summer periods of natural river flows at or below the long-term average.

F. RELATIVE CONTRIBUTIONS OF INDIVIDUAL RATES TO SIMULATED DO

We evaluated the relative contribution of the input DO, as well as those of the physical and biological processes in the river reach, to the DO concentration in the most downstream element of the reach (where DO would indicate the cumulative effects of all upstream sources and sinks of oxygen).

Accordingly, to quantify those individual contributions, we calculated the average DO concentration in this segment for validation runs under two different natural river flows (Table III-3): 27-28 June 1981 (23,057 cfs) and 25 July-2 August 1981 (13,065 cfs). As expected, the relative dominance of the input DO is larger for the higher flow period. In addition, we calculated the relative contributions to the

output DO of each constituent process. The results indicate that the portion of downstream DO which is due to the DO of the discharge dominates the total, even for the time interval characterized by shutdown periods (< 1,000 cfs, when input DO would be expected to have little effect). The individual contributions of benthic community respiration, and the production and respiration of the water-column community, do not account for more than 10% of the DO of water leaving the segment.

We calculated these individual contributions by running the model with a different term set to zero in each of several runs, and by calculating the percentage differences from the standard run. Because of small higher-order effects (e.g., feedback in the reaeration term; parameter interactions), the tabled percentages do not sum to 100%.

Among the in situ biological and physical processes, benthic community production shows the largest contribution, and is twice as important during the lower flow period than under high flow.

The relative contribution of reaeration is much larger for the low flow period than for high river flows. However, a large part of this apparent difference can be ascribed to larger input DO values for the first vs. the second period (Figs. III-15b vs III-16b), since reaeration is driven in part by the saturation deficit.

Benthic community respiration, and the production and respiration of the water-column community, never individually change the total DO concentration more than 10%.

The relative contributions of the terms in Table III-3 are long-term averages over the full range of discharges. To quantify the effects of discharge volume on their relative contributions to oxygen flux, we sorted the data from the 25 July - 2 August model run into four discharge categories. The results indicate that the input DO concentration increases in dominance with increasing discharge -- ranging from 66% at discharges less than 2,000 cfs to 85% at 30,000 cfs. The relative contributions

of in situ processes to DO in the downstream segment decrease with increasing discharge, as was observed for the relationships of the processes to natural river flow. In general, it appears that discharge DO contributes at least 90% of the total DO at discharges above 28,000-40,000 cfs (when water residence times in the reach are 2 hours or less). Reaeration causes most of the remaining changes in DO.

Conversely, during shutdown periods (e.g. less than 2,000 cfs), respiratory processes consume, on average, an amount of oxygen equal to 18% of the output oxygen. However, these averages also include daytime shutdown periods in which the production terms are also large. If the averages were done for nighttime shutdowns alone, the relative importance of the respiratory processes would undoubtedly increase. If accurate estimates of fish respiration were added to the model, it is possible that the three respiratory terms would control DO during nighttime shutdown periods.

G. SENSITIVITY ANALYSIS

The model uses a large number of parameters for rate processes and inputs in simulating DO distributions in the river reach. It is useful at this point to assess the relative importance of these parameters to the accuracy and precision of the results, and to examine the quality and representativeness of data used to estimate some of the parameters. It is also useful to determine whether discrepancies between observed and simulated DO values occur that are caused by factors not accounted for in model structure. In this section, we attempt to quantify the sensitivity of the DO output from the model (e.g., simulated DO values at Transect A) to variations in individual rate processes affecting DO, and to some of the unpredictable physical inputs to the system that affect these processes (e.g., light intensity, input water temperature and DO, and turbidity).

To examine the effects of such variations on simulated downstream DO values, we artificially varied each individual rate process and some inputs (Tables III-4 and III-5, respectively) in a series of simulations of the 25 July-2 August 1981 time interval previously used for validation (Fig. III-16). We multiplied each of the rate processes in Eq. 4 (Table III-4) by 0.5 and by 1.5 (factors much larger than the variations expected in the real system) in separate runs and calculated the average change in DO (ppm) relative to the standard run (Fig. III-16c). The rate processes of Table III-4 are arranged in order of decreasing sensitivity to these changes. The averages cover all nine days of the runs, and thus include the full range of discharges released by the turbines. We did not attempt to describe sensitivities as functions of discharge. Also, the sensitivities of water-column and benthic production are underestimated when calculated as full-day averages, since the averages include nighttime periods when these rate processes are near zero.

Model DO output is most sensitive to benthic metabolism rates (Table III-4). This sensitivity may contribute to the poor fit of the model output DO to field data under certain conditions. For instance, during shutdown periods, simulated DO values are often larger than those observed at transect A (e.g., Figs. III-13c and III-16c) for reasons relating to benthic metabolism in pools, as discussed in the calibration section of this report.

Atmospheric reaeration rates also affect model output significantly (Table III-4). Our inability to measure the rate coefficient at high discharges forced us to use a relationship derived from data from several empirical studies in which conditions may not have been comparable to those in the Susquehanna River. We are presently unable to further assess the accuracy of the reaeration rate estimates used in the model. However, some qualitative observations indicate that the rate is reasonably accurate. Reaeration (Eq. 7) is a negative feedback process, which tends to restore high or low DO values toward the

Table III-4. Sensitivity of simulated output DO to artificial variations of oxygen rate processes

Rate Process	Term in Equation 4	Change Factor	Mean ΔDO (ppm)	Variance ΔDO
Benthic production	P_b	x 0.5	-0.45	0.33
		x 1.5	+0.44	0.31
Atmospheric reaeration	K_2 (C*-C)	x 0.5	-0.34	0.06
		x 1.5	+0.27	0.04
Benthic respiration	R_b	x 0.5	+0.29	0.02
		x 1.5	-0.29	0.02
Water-column production	DP_{wc}	x 0.5	-0.23	0.04
		x 1.5	0.23	0.04
Water-column respiration	R_{wc}	x 0.5	+0.11	0.002
		x 1.5	-0.11	0.002

saturation value (7-8 ppm for the summer temperatures of the periods simulated for calibration and validation). If the model's reaeration rate were too high, extreme supersaturated conditions (i.e., daytime DO peaks during shutdowns) or undersaturated conditions (i.e., nighttime DO minima) would be rapidly corrected by the reaeration mechanism, forcing a convergence on the saturation value. If the reaeration rate were too low, the model could not reproduce occasional nighttime increases in DO, which can be due only to reaeration. We thus feel reasonably confident in the reaeration mechanism used in the model.

Output DO levels appear to be the least sensitive to metabolic rates in the water column (Table III-4). Measurements of these rates were subject to some uncertainty, both because they were small in magnitude (near the detection limit of the method used) and because they were very variable in space and time (Philipp and Klose 1981). Thus, the least certain of our estimated rate processes also proved to have the smallest effect on the accuracy of our simulated results. Any errors in estimating water-column light intensities would thus have minimal effect on simulated DO levels. During shutdown periods, when DO impacts on biota are likely to be largest, the water volume in the river is near its minimum. This further decreases the effect of water-column rate processes on the total DO of the river at such times. Thus, inaccuracies in the estimation of water-column processes are not likely to significantly affect DO in the river reach.

The magnitude of the ΔDO values of Table III-4 can also be compared to the overall mean DO of the 9-day run -- 5.8 ppm. Variations of the individual rates were ± 50% about the values used in the standard run. The maximum effect on output DO from any of these variations was ± 8% (due to benthic production). This indicates that, when averaged over all river conditions over many days, in situ processes have a relatively small effect on average DO levels in the river. However, this first-order sensitivity analysis neglects high-order effects, so the effects

of changes in individual parameters cannot be superimposed to estimate the sensitivity of the total system. Also, this average sensitivity (over 9 days) may not be appropriate for evaluating available habitat, which is controlled by the most stringent conditions encountered over a period of time (e.g., shutdown periods).

Besides the rate processes described above, a number of system inputs also affect model behavior. First, simulated output DO values are very sensitive to input DO concentrations. The addition or subtraction of 1 ppm to input DO concentrations (Table III-5) produces a ±0.7-ppm average change in DO at the fall line. This 9-day average hides the fact that the importance of input DO increases in proportion to discharge (i.e., input oxygen is determined by $Q \times C_{in}$ in Eq. 4). We are currently undertaking an intensive analysis to estimate errors in measuring the DO concentration of the discharge water. The sensitivity runs also point out the importance of identifying the effects of reservoir processes on discharge DO, especially the prediction of discharge DO values under any future continuous discharge regime.

Next, factors controlling production (surface light intensity and Secchi-disk depth) also have a relatively large effect on output DO values (Table III-5). Most of the resulting changes in DO are probably due to the effects of ambient light intensity on benthic rather than water-column productivity.

Lastly, water temperature affects all five oxygen rate processes (Table III-4), so its correct estimation is important. The sensitivity runs (Table III-5) indicate that a ±5°C change of input water temperature (~ 25°C during summer) does change DO values by up to 0.5 ppm. Since actual temperatures of input water are relatively constant over long periods in summer, 5°C errors in its estimation are not likely to occur. Downstream, however, 5°C temperature increases are not uncommon, especially during periods with low discharges. These could increase daytime rates in pools, a process which may be reflected in large

Table III-5. Sensitivity of simulated output DO to artificial variations of system inputs

Input	Parameter (model equation)	Change	Mean ΔDO (ppm)	Variance ΔDO	Maximum ΔDO	Minimum ΔDO
Input DO concentration	C_{in} (Eq. 4)	-1.0 ppm	-0.73	0.03	0.0	-0.95
		+1.0 ppm	+0.73	0.03	+0.95	0.0
Light intensity at water surface	I_o (Eq. 11, both benthic and water-column P)	x0.5	-0.41	0.18	--	--
		x1.5	+0.17	0.06	--	--
Secchi disk depth	z_{Secchi} (Eq. 13)	1.0 m	-0.38	0.11	--	--
		1.7 m	Standard run			
		2.5 m	+0.17	0.02	--	--
Input water temperature	T (Eqs. 9, 10, 14)	x0.8	+0.23	0.43	1.27	-1.50
		x1.2	-0.49	0.38	1.13	-1.58

DO increases during daytime shutdown periods (Figs. III-11 and III-14). Since the model does not include a detailed heat budget, it is unlikely that its temperature mechanism (Appendix B) can be improved.

H. DISCUSSION

The previous sections show that the model generally simulates summertime conditions over a wide range of discharges. However, the fit of the model's DO output to observed data is poorest for conditions when the turbines are shut down. Under such conditions, the assumption of complete mixing within a segment may be violated, so that no single point estimate of DO may be representative of the DO distribution in a segment. Otherwise, the model can be used to assess the change in DO distributions due to biological and physical sources and sinks of oxygen within the river reach.

The validation runs indicate that the DO of the turbine discharge dominates the oxygen output of the system at the fall line, and that this relative dominance increases with increasing daily river flow and/or shorter-term discharge volume. Benthic metabolism contributed the most to the in situ oxygen change, followed by reaeration. Water-column community metabolism was of minor importance.

We also assessed the sensitivity of the model's DO output to artificial variations of rate processes or individual parameters. The sensitivity analyses showed that variations in the rates of benthic production and reaeration had the largest effects on the model's output. Despite the paucity and/or poor quality of field data on these rates as functions of space and time, the model usually reproduces observed temporal and spatial DO distributions. In contrast, the model's output appears relatively insensitive to changes in water-column metabolism, so errors in estimating these rates should have relatively little effect on model accuracy.

The model's output is also sensitive to the DO concentration of the turbine discharge water. This dependence of the model on input values, the present uncertainty about the accuracy of turbine DO data used as DO input to the model, and our present lack of knowledge about the dependence of the DO of the discharge water on reservoir processes and discharge volume, all indicate the need for further analyses to determine the source of the discharge water within the reservoir and the effects of water withdrawal from the reservoir on DO distributions near the dam. We are currently beginning such analyses. They include mechanistic simulation modeling to describe the causes of observed DO distributions in the reservoir; analyses to describe the withdrawal of water from the reservoir; and time-series analyses of the DO data from the turbine cooling line (data that are presently used as DO input to the model) relative to reservoir DO data, to generate a more precise means of estimating the DO of discharge water. When these analyses are completed, the river DO model will be a versatile tool for estimating downstream DO distributions in summer under a variety of river flows and turbine operating schedules (e.g., hypothetical minimum discharge regimes). In the meantime, the model can still be used to make relative comparisons among the downstream DO distributions resulting from hypothetical modifications of dam operations.

IV. LITERATURE CITED

Bennett, J.P., and R.E. Rathbun. 1972. Reaeration in open-channel flow. U.S. Geological Survey Professional Paper No. 737. Washington, DC.

Boynton, W.R., W.M. Kemp, C.G. Osborne, and K.R. Kaumeyer. 1978. Metabolic characteristics of the water column, benthos and integral community in the vicinity of Calvert Cliffs, Chesapeake Bay. Volume I. Maryland Power Plant Siting Program Report No. 2-72-02 (77). Annapolis, MD.

Carter, W.R., III. 1973. Ecological study of Susquehanna River and tributaries below the Conowingo Dam. National Marine Fisheries Service. Federal Aid Project Report No. AFSC-1. Maryland Department of Natural Resources, Fisheries Administration, Annapolis, MD.

Copeland, B.J., and W.R. Duffer. 1964. The use of a clear plastic dome to measure gaseous diffusion rates in natural waters. Limnol. Oceanogr. 9:494-499.

Davis, J.C. 1975. Minimal dissolved oxygen requirements of aquatic life with emphasis on Canadian species: A Review. J. Fish. Res. Board Can. 32:2295-2332.

HEC (Hydrologic Engineering Center). 1977. Gradually varied unsteady flow profiles. U.S. Army Corps of Engineers, Davis, CA.

Jackson, D.R., and A.K. Karplus. 1979. Hydrologic studies of effects of Conowingo Dam. Susquehanna River Basin Commission Technical Report No. 1. Harrisburg, PA.

Jackson, D.R., and G.J. Lazorchick. 1980. Instream flow needs study, Susquehanna River, vicinity of Conowingo Dam. Susquehanna River Basin Commission Technical Report No. 2. Harrisburg, PA.

Janicki, A.J., and R.N. Ross. 1982. Benthic invertebrate communities in the fluctuating riverine habitat below Conowingo Dam. Report prepared for Maryland Power Plant Siting Program by Martin Marietta Environmental Center, Baltimore, MD.

Kester, D. 1975. Dissolved gases other than carbon dioxide. In: Chemical Oceanography I, pp. 497-556. J.P. Riley and G. Skirrow, eds. London: Academic Press.

Kremer, J.N., and S.W. Nixon. 1978. A Coastal Marine Ecosystem: Simulation and Analysis. Berlin: Springer-Verlag.

Krenkel, P.A., and V. Novotny. 1980. Water Quality Management. New York: Academic Press.

Levenspiel, O., and W.K. Smith. 1957. Notes on the diffusion type model for the longitudinal mixing of fluids in flow. Chem. Eng. Sci. 6:227-233.

Nixon, S.W., C.A. Oviatt, J.N. Kremer, and K. Perez. 1979. The use of numerical models and laboratory microcosms in estuarine ecosystem analysis--simulations of a winter phytoplankton bloom. In: Marsh-Estuarine Systems Simulation, pp. 165-188. R.F. Dame, ed. Columbia, SC: University of South Carolina Press.

Parsons, T.R., and M. Takahashi. 1973. Biological Oceanographic Processes. New York: Pergamon Press.

Petrimoulx, H.J., and P.N. Klose. 1981. Resident fisheries study, lower Susquehanna River, Maryland. Maryland Power Plant Siting Program Report No. PPSP-UBLS-81-5. Annapolis, MD.

Philipp, K.R., and P.N. Klose. 1981. Lower Susquehanna River oxygen dynamics study. Maryland Power Plant Siting Program Report No. PPSP-UBLS-81-4. Annapolis, MD.

Phinney, H.K., and C.D. McIntire. 1965. Effect of temperature on metabolism of periphyton communities developed in laboratory streams. Limnol. Oceanogr. 10:341-344.

Photo Science, Inc. 1980. Operational effects of Conowingo Dam on the Susquehanna River. Report to the Susquehanna River Basin Commission, Gaithersburg, MD.

Potera, G.T., K.R. Philipp, T.D. Johnson, H.J. Petrimoulx, and P.N. Klose. 1982. Lower Susquehanna River hydrographic and water quality study, summer 1981. Maryland Power Plant Siting Program, Annapolis, MD.

Radiation Management Corp. In preparation. Report of results of 1980 studies of DO and temperature in the vicinity of Conowingo Dam. Drumore, PA.

Roques, P., and S. Nixon. In preparation. Direct measurement of air-water gas exchange coefficient with special reference to oxygen. University of Rhode Island, Graduate School of Oceanography, Kingston, RI.

Smith, D.J. 1978. Water quality for river-reservoir systems. Hydrologica Engineering Center, U.S. Army Corps of Engineers, Davis, CA.

Steele, J.H. 1965. NOtes on some theoretical problems in production ecology. In: Primary Productivity in Aquatic Environments, pp. 383-398. C.R. Goldman, ed. Mem. Ist. Ital. Idrobiol., 18 Suppl. Berkely, CA: Univeristy of California Press.

Streeter, H.W., and E.M. Phelps. 1925. A study of the pollution and natural purification of the Ohio River. U.S. Public Health Service, Public Health Bull. 146. Washington, DC.

Strickland, J.D.H., and T.R. Parsons. 1968. A practical handbook of seawater analysis. Fisheries Research Board of Canada Bulletin No. 167. Ottawa.

Sverdrup, H.U., M.W. Johnson, and R.H. Fleming. 1942. The Oceans. Englewood Cliffs, New Jersey: Prentice-Hall.

Wetzel, R.G. 1975. Limnology. Philadelphia: W.B. Saunders.

Yen, B.C. 1979. Unsteady flow mathematical modeling techniques. In: Modeling of Rivers, H.W. Shen, ed. New York: Wiley-Interscience.

APPENDIX A

SATURATED DO CONCENTRATION OF WATER (FROM KESTER 1975)

APPENDIX A

SATURATED DO CONCENTRATION OF WATER (FROM KESTER 1975)

$$\ln C = 173.9894 + 255.5907 \frac{100}{T} + 146.4813 \ln \frac{T}{100} - 22.2040 \frac{T}{100}$$

(Eq. A-1)

where:

C = solubility of oxygen in fresh water ($\mu m/kg$)

T = temperature (°K) (°K = °C + 273.15)

$C \times .032 = (O_2)_{sat}$, mg O_2/kg

APPENDIX B

ESTIMATION OF DIEL TEMPERATURE CHANGES IN RIVER SEGMENTS

APPENDIX B

ESTIMATION OF DIEL TEMPERATURE CHANGES IN RIVER SEGMENTS

Downstream changes in temperature can be estimated by the following equations:

$$T = a_o + a_1 + a_2 \sin \frac{2\pi}{24} (t + \tau) \qquad \text{(Eq. B.1)}$$

where:

T = temperature at transect A at flow ≅ 3,000 cfs (a function of time)

a_o = average temperature of water discharged from turbines

a_1 = diel average difference in temperature between water at transect A and at the turbine discharge (depends on discharge, and difference between air and water temperature)

a_2 = amplitude of diel temperature oscillation about a_1

t = time of day, in decimal hours

τ = lag (decimal hours after midnight) of beginning of sine oscillation.

Using data from a low discharge (≈ 3,000 cfs) period (12-14 July 1980), a nonlinear regression computed the following temperature equation for transect A:

$$T = 26.8 + 1.0 + 3.5 \sin \frac{2\pi}{24} (t - 9.96)$$

$$(F_{3,192} = 1359., P < .0001, R^2 = .96) \qquad \text{(Eq. B.2)}$$

The average temperature of water discharged by the turbines (a_o) depends on the history of the water accumulated in Conowingo Reservoir (e.g., its flow rate and solar heating during passage from the upstream watershed). The diel average temperature change of water in the reach below Conowingo Dam (a_1) depends on the discharge rate and on the difference between air and water temperature. During periods of summary low river flow (conditions of most interest for this study) values for a_o and a_1 are likely to be close to those estimated from the July 1980 data.

The amplitude of diel heating and cooling of river water (a_2) is largest when water residence time upstream of transect A is large and when water volume is small relative to surface area (through which heat exchange occurs). Thus, temperatures fluctuate most under shutdown or low discharge conditions, when the volume:surface-area ratio is small (i.e., water depth is small) and water travel time in the river reach is large.

To reduce this temperature fluctuation for high discharges (which decrease residence times), the amplitude term was made inversely proportional to depth and time-of-travel, for discharges less than 40,000 cfs:

$$a_2 = \frac{65378.}{\text{depth} \times \text{time of travel}} \qquad \text{(Eq. B.3)}$$

where depth is the local water depth (ft), as computed by USTFLO and time-of-travel (s) was computed from a nonlinear regression of times-of-travel vs. 13 steady-state flows between 1,000 and 65,000 cfs (from USTFLO simulations):

$$TOT = 14{,}146 + 2.9 \times 10^7/Q - 0.159Q \qquad \text{(Eq. B.4)}$$

In the DO model, Eq. B.4 was substituted into B.3, which in turn was used by Eq. B.2 to estimate temperature at transect A. Temperatures at upstream transects were estimated by decreasing a_1 and a_2 in proportion to the distance of the transect from the dam.

APPENDIX C

REGRESSION OF WATER COLUMN RESPIRATION VS. TEMPERATURE

APPENDIX C

REGRESSION OF WATER COLUMN RESPIRATION VS. TEMPERATURE

$R_{WC} = 0.01 + 0.0016\ T$

$F_{1,87} = 7.86$ $\quad Pr\ (F > 7.86) = 0.006$ $\quad R^2 = 0.10$

APPENDIX D

REGRESSION OF BENTHIC RESPIRATION VS. TEMPERATURE

APPENDIX D

REGRESSION OF BENTHIC RESPIRATION VS. TEMPERATURE

$$R_B = - 0.016 + 0.0048T$$

$F_{1,34} = 5.48$ $\quad Pr\ (F > 5.48) = 0.025$ $\quad R^2 = 0.14$

APPENDIX E

CALCULATION OF SOLAR RADIATION AT THE WATER SURFACE FROM ASTRONOMICAL AND METEOROLOGICAL INFORMATION

APPENDIX E

CALCULATION OF SOLAR RADIATION AT THE WATER SURFACE FROM ASTRONOMICAL AND METEOROLOGICAL INFORMATION

E.1. CALCULATION OF SUN ANGLE AS A FUNCTION OF DATE, TIME, AND LOCATION

The following FORTRAN subroutine yields the solar elevation angle (radians):

```
      SUBROUTINE SUN (IYR, IDAY, IND, HR, C)
      COMMON/ALL/
                                                  COMMENTS

      DIMENSION IDFAC (12,2)
      DATA CONST/57.29578                  * degrees/radian = 180/π

      DATA IDFAC/0,31,59,90,120,           * Julian day number of the last
        151,181,212,243,273,304,             day of the previous month
        334,0,31,60,91,121,152,              (normal, leap years)
        182,213,244,274,305,335/

C               ALAT = latitude (degrees) = 39.5

C              ALONG = longitude (degrees) = 76.2

C               Zone = time zone (GMT-LST)

C                    i.e., Atlantic = 4
                           (or Eastern Daylight)

C                          Eastern = 5

C                          Central = 6

C                 HR = hour of day (LST)

C                IYR = last two digits of year

C               IDAY = number of days in month

C                IMO = month number

      DUM = ALT/CONST                      * transform latitude into
                                             radians

      SINLAT = SIN(DUM)                    * sine of the latitude

      COSLAT = COS(DUM)                    * cosine of the latitude
```

```
      TEMPZ = 15.*ZONE-ALONG              * calculate longitude posi-
                                            tion from central time
                                            zone meridian (360/24 = 15)
C     Check for leap year
       LYS = 1

      IF[MOD(IYR,4).EQ.0]LYS = 2          * in leap year

C     Calculate Julian day number
       DAYl=IDAY+IDFAC(IMO,LYS)

C     Determine the angular fraction (degrees) of the year,

C     SIGMA, measured from the vernal equinox, for this date

           DAYNO = (DAYI-1.0)*360./365.242/CONST

          TDAYNO = 2.*DAYNO

            SIND = SIN(DAYNO)

            COSD = (DAYNO)

           SINTD = SIN(TDAYNO)

           COSTD = COS(TDAYNO)

C     Account for ellipticity of orbit

           SIGMA = 279.9348+(DAYNO*CONST)+1.914827*SIND
                  -0.079525*COSD+0.019938*SINTD
                  -0.00162*COSTD

C     Calculate the sine of the solar declination

            DSIN = SIN(23.44383/CONST)*SIN(SIGMA/CONST)

                                        * equivalent to SINδ = SIN
                                          of obliquity*SIN of
                                          longitude of sun

            DCOS = SQRT(1.0-DSIN*DSIN)  * COSINE of solar declination


C     Determine time (hours,LST) of solar noon

             AMM = 12.0+0.12357*SIND-0.004289*COSD+0.153809
                  *SINTD+0.060783*COSTD

C     Determine solar hour angle (radians) measured from "solar noon"

              HI = [360./24.*(HR-AMM)+TEMPZ]/CONST
```

```
C   Calculate SINE of the solar elevation angle
      SINALF = SINLAT*DSIN+DCOS*COSLAT*COS(HI)
C   Calculate solar elevation angle (radians)
      ALF = ATAN2[SINALF,SQRT(1.-SINALF*SINALF)]
```

E.2. ESTIMATION OF CLEAR-SKY RADIATION

The following equation (Sverdrup et al. 1942; Kremer and Nixon 1978) estimates clear-sky radiation based on solar elevation angle:

$$I_{clear} = S_1^{-Ta_m\, m} \sin(h) + D$$

where S = solar constant (1.94 ly/min)

T = atmospheric turbidity factor

a_m = clear-sky extinction coefficient = 0.128 - - 0.064 log(m)

m = relative atmospheric path length = 1/sin(h)

h = sun angle (degrees)

D = diffuse radiation component

= 0.44 exp (-0.22h)

The predicted clear-sky maximum is adjusted for cloudiness using National Weather Service's surface cloud-cover data:

$$I = I_{clear} (1.0 - 0.017\ C)$$

where C = cloud cover (tenths)

Finally, from a regression to actual data:

$$I_o = 0.7\ I$$

APPENDIX F

NON LINEAR REGRESSIONS FITTING WATER-COLUMN METABOLISM DATA TO THE STEELE (1965) EQUATION (Eq. 11)

APPENDIX F

NONLINEAR REGRESSIONS FITTING WATER-COLUMN METABOLISM DATA TO THE STEELE (1965) EQUATION (Eq. 11)

$$P = P_{max}\, I_{opt}^{I}\, e^{(1 - I/I_{opt})}$$

Data	P_{max}	I_{opt}	regression F	regression P	R^2
All temperatures	0.0023**	0.153**	47.2	<0.001	0.52
T ≤ 25°	0.0020**	0.200**	28.4	<0.001	0.50
T > 25°	0.0054**	0.131**	51.3	<0.001	0.78

** P < 0.01

NOAA COASTAL SERVICES CTR LIBRARY
3 6668 14110932 4